Article

Abyssal Peridotite as a Component of Forearc Mantle: Inference from a New Mantle Xenolith Suite of Bankawa in the Southwest Japan Arc

Shoji Arai [1,*], Akihiro Tamura [1], Makoto Miura [1,2] and Kazuma Seike [3]

[1]   Department of Earth Sciences, Kanazawa University, Kanazawa 920-1192, Japan; aking826@gmail.com (A.T.); makomiu1214@gmail.com (M.M.)
[2]   Gemological Institute of America (GIA) Tokyo Godo Kaisha, Tokyo 110-0016, Japan
[3]   Saitama Museum of Natural History, Nagatoro 1417-1, Nagatoro-machi, Chichibu-gun, Saitama 369-1305, Japan; ks-cetolith@ruri.waseda.jp
*   Correspondence: ultrasa@staff.kanazawa-u.ac.jp; Tel.: +81-76-264-6521

check for updates

Abstract: Lithology and petrologic nature of the forearc mantle have been left unclear due to the very limited sampling to date. Here, we present petrological data on a forearc peridotite suite obtained as xenoliths in an alkali basalt dike (7.5 Ma) from the Bankawa area in the Southwest Japan arc for our better understanding of the forearc mantle. The host alkali basalt is of asthenosphere origin, and passed through a slab window with slight chemical modification by the slab-derived component. The Bankawa peridotite suite is comprised of lherzolites, which contain various amounts of secondary phlogopite and were metasomatized to various degrees. The least metasomatized lherzolite exhibits Fo_{91} of olivine, $Cr/(Cr + Al) = 0.3$ of chromian spinel, and depletion of middle to light rare-earth elements in clinopyroxene, and is overall similar to an abyssal lherzolite. It had originally formed at the proto-Pacific Ocean and then was trapped at a eastern margin of Eurasian continent by initiation of subduction. The forearc mantle peridotite formed as a residue of proto-arc magma formation is depleted harzburgite as represented by the peridotites obtained from the forearc seafloor, but can be less depleted abyssal peridotite if being devoid of partial melting or reaction with magmas after entrapment.

Keywords: forearc mantle; lherzolite xenoliths; abyssal peridotite; alkali basalt; Bankawa; Southwest Japan arc

1. Introduction

One of the characteristics of the subarc mantle is heterogeneity both in chemistry and in lithology [1,2]. The number of localities of mantle xenoliths is very small from arc areas as compared with other settings [3,4], and this leads to a difficulty in obtaining a detailed picture of the lower crust and the upper mantle of arcs, which essentially have complicated tectonic histories [4–6]. Some supra-subduction zone ophiolites indicate a complicated evolution history of arcs. The Oman ophiolite, for example, record switch of tectonic setting from mid-ocean ridge (spreading) to arc (subduction) [7–9], and its mantle section is mainly composed of abyssal peridotite [10], which has been in part converted to depleted arc peridotite [11]. We expect therefore that the abyssal peridotite has been trapped and preserved in a mantle wedge, especially in its forearc part, during the arc evolution process. Mantle peridotite xenoliths relatively abundant in Cenozoic volcanics of the rear side of arcs such as the Northeast and Southwest Japan arcs [1,2,4,12–16] (Figure 1). Mantle peridotite xenoliths from several recent volcanoes located at volcanic front supply us with information on the lithospheric

mantle beneath the front [17–19]. Forearc mantle peridotites have been obtained from the ocean floor of trench area through dredging, drilling and submersible dive [20–23]. Those peridotites recovered near the trench may be representative of a near-edge part of the mantle wedge. Both the edge and the volcanic front sides of the lithospheric mantle wedge have been considered to be mainly composed of depleted peridotites, i.e., harzburgites [6]. The other part of the lithospheric mantle wedge, however, has not been sampled as xenoliths, and its composition has been left unclear. The Bankawa ultramafic xenolith suite transported by an alkali basalt (7.5 Ma) [24] from southern Osaka (Kii Peninsula), the Southwest Japan arc, was derived from the forearc mantle (Figure 1), and serves as a probe into a portion of the mantle wedge. This greatly contributes to our better understanding of the petrologic structure and evolution of the mantle wedge.
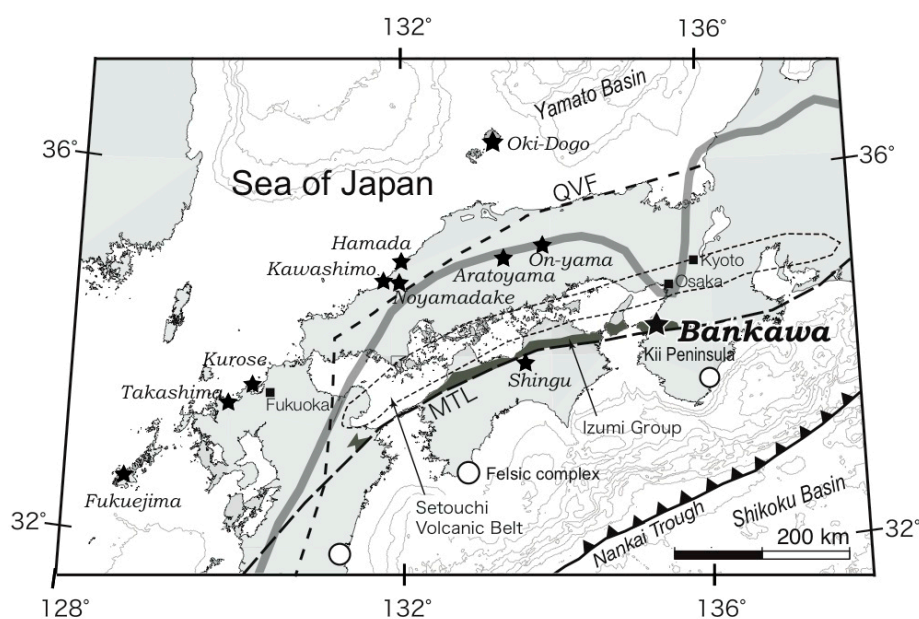
Figure 1. Location of the Bankawa outcrop in the Kii Peninsula, southwestern Japan. Main mantle xenolith localities (black star) are after Arai et al. [15]. Distributions of the Setouchi Volcanic Belt and felsic complexes (open circle) [25] and the Izumi Group [26] are shown. QVF and MTL are Quaternary volcanic front and Median Tectonic Line [27], respectively. Note that Bankawa is one the most Pacific-ward localities of mantle xenoliths in the SW Japan arc. The position of the edge of the slab (Philippine Sea plate) (thick gray line) is after Nakajima and Hasegawa [28].

The Japanese islands have been situated on subducting oceanic plates since the Mesozoic (or earlier) except for the period of the opening of the Shikoku Basin (27–15 Ma) [19]. The upper mantle beneath Bankawa has been therefore part of the mantle wedge of the SW Japan arc.

All the alkali basalts that carried peridotitite xenoliths are younger than 11 Ma [29] except for the Shingu lamprophyre (Figure 1), which is 17 Ma in age [30]. They erupted before the Philippine Sea plate, which started subduction in Miocene (17 Ma), reached beneath each place [27,31]. Alkali basalt magmatism of Miocene has not been found in the Kii Peninsula of the SW Japan arc, which was widely underlain by the subducted plate at that time [27,31]. Origin of the Bankawa alkali basalt (7.5 Ma) is thus enigmatic in origin. Petrological and chemical characteristics of the host basalt are also described because Bankawa is a new locality of peridotite xenolith-bearing basalt and they have not been reported in detail. This study will also contribute to our understanding of the peculiar Cenozoic magmatism in the SW Japan arc [27,31,32].

2. Geologic Outline

Intrusive basaltic rocks were found in the western Izumi Mountains of the south Kinki distinct, Southwest Japan [28]. The Izumi Mountains run across Osaka and Wakayama Prefectures in the Kii

Peninsula. An alkali basaltic dike, exposed along Bankawa River, contains a lot of peridotite xenoliths, less than 10 cm across (Figure 2). The Bankawa outcrop (34.2920° N, 135.1930° E) is located in Tannowa, Misaki Town, southern Osaka, Japan.

Figure 2. Photographs showing the mode of occurrence of peridotite xenoliths at Bankawa, Japan. The coin is about 2.3 cm across. (**a**) altered lherzolite xenolith (L) in the marginal breccia zone of the alkali basaltic dike; (**b**) fresh lherzolite xenolith (L) in massive alkali basalt.

In the Izumi Mountains, four geologic divisions, namely the late Pliocene–early Pleistocene Osaka Group, Cretaceous Ryoke granitoids and Sennan Rhyolites, Late Cretaceous Izumi Group, and Sanbagawa metamorphic belt, have been established from north to south [26,33]. The Izumi Group unconformably caps or is bounded with faults by the Ryoke granitoids and Sennan Rhyolites in the northern margin, and is in contact with a great boundary fault, the Median Tectonic Line (MTL), in the southern margin. The Sanbagawa metamorphic belt derived from a Cretaceous accretionary complex lies in the south of the MTL. The Osaka Group unconformably overlies the Ryoke granitoids, Sennan Rhyolites and the Izumi Group. In the western part of the Izumi Mountains, the Izumi Group forms a major asymmetrical syncline named the Kyoshi Syncline [34]. Some Miocene intrusive or plutonic rocks were reported at a northern margin of the Izumi Mountains as well as along the MTL [35].

The alkali basaltic dike cuts sedimentary rocks of the Izumi Group, which are composed of predominant alternating beds of sandstone and mudstone, and rare thick mudstone strata interbedded with thin conglomerate layers. The dominant strata at this site generally strike N–S to N20° W, dip 30° to 50° to the East. The Bankawa outcrop is just in the axial zone of the Kyoshi Syncline. This horizon can be correlated with the lower part of the Shindachi Formation (lithologic units Ss4 and Ss5) on the basis of lithological studies [36]. The Shindachi Formation has been considered to be of Maastrichtian age based on ammonoid biostratigraphy [37] and was dated by a fission track method at 70.9 ± 3.4 Ma [33].

We recognized the alkali basaltic dike extending over a distance of 50 m in the west–east direction along both Bankawa River and forest trails, and the thickness is less than a few meters. The alkali basaltic rocks thermally metamorphosed sandstone or mudstone of the Izumi Group adjacent to the dike. Massive basalt is alternated with breccias from west to east in the dike. A K-Ar age of

7.5 Ma was obtained on sanidine crystals of the basalt [28]. This is almost the same as the age of the Noyamadake basanite, 7.4 Ma [29], which also contains mantle xenoliths [1,38], and is in the temporal range (0.1–17 Ma; mostly < 11 Ma) of other mantle-xenolith bearing Cenozoic basalts in SW Japan [15].

3. Petrography

The host alkali basalt is massive, black in color on fresh surface, fine-grained and homogeneous, and contains amygdules filled with chabazite or calcite. Fresh peridotite xenoliths, less than 10 cm across, were found in the massive part (Figure 2b). The volcanic breccias enclose semi-angular fragments, up to tens of centimeters in size, of sandstone, basalt, and rarely mudstone and altered peridotites (Figure 2a). The host rock is sparsely phyric, containing phenocrysts of clinopyroxene and olivine less than 1 mm across (Figure 3a). The groundmass is fine-grained and composed of feldspars (sanidine and plagioclase), clinopyroxene, olivine (mostly altered) and mesostasis. Feldspathoids were not found even though carefully searched under the microscope. The peridotite xenoliths show sharp contact with the host rock except along orthopyroxenes where fine-grained reaction products [39] were formed in between (Figure 3a).
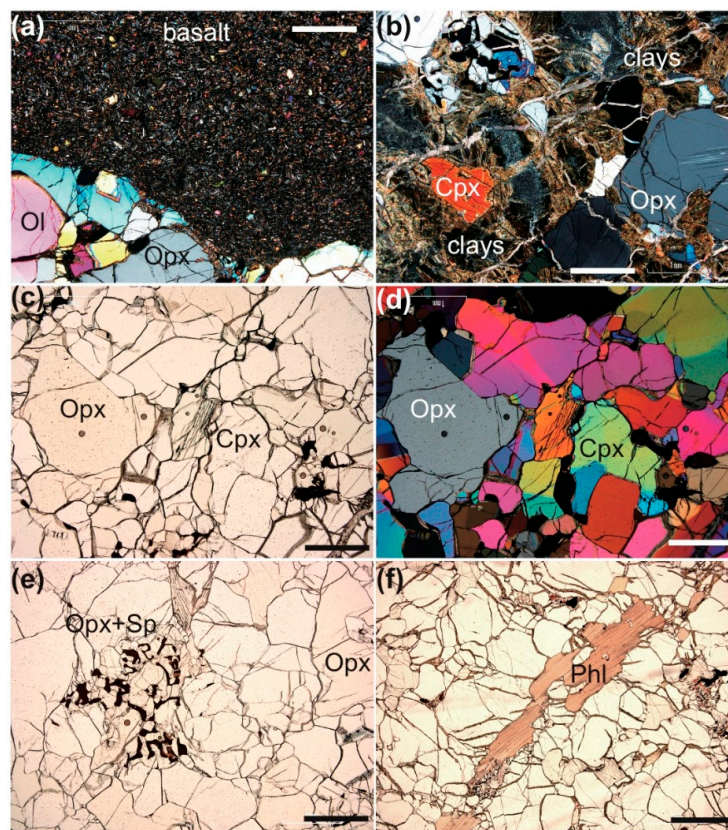
Figure 3. Photomicrographs. (**a**,**b**,**d**) by crossed-polarized light. (**c**,**e**,**f**) by plane-polarized light. Scale bar is 1 mm. Abbreviations; Ol, olivine: Opx, orthopyroxene: Cpx, clinopyroxene: Sp, chromian spinel: Phl, phlogopite. (**a**) Lherzolite xenolith (lower) in sparsely phyric alkali basalt. Note a thin reaction zone between orthopyroxene and the host basalt. No. IZS-1; (**b**) altered lherzolite (IZS-6). Olivine has been completely altered to clays. Note thin clinopyroxene lamellae in the core of orthopyroxene; (**c**,**d**) Prortogranular texture of lherzolite (IZS-1); (**e**) vermicular aggregate of chromian spinel and orthopyroxene in lherzolite (IZS-3); (**f**) phlogopite veinlet mainly replacing olivine in lherzolite (IZS-12).

The peridotite xenoliths are relatively fine-grained and show protogranular to weakly porphyroclastic textures (Figure 3). They are of Group I [40]; they appear compact and contain greenish clinopyroxene (chromian diopside). Neither Group II xenoliths, which are black clinopyroxene-bearing and coarse-grained, nor related megacrysts were found from Bankawa. Most of the xenoliths are

slightly clinopyroxene-poor lherzolites, but some are poor in pyroxenes possibly due to the small size (Figure 2) and heterogeneity of the xenoliths. Modal compositions were determined by chemical mapping with EPMA (see Section 4.2 below) on the thin section. A typical modal composition is 71.5% olivine, 21.9% orthopyroxene, 5.5% clinopyroxene and 1.1% chromian spinel. Olivines vary in size from several mm to <1 mm across, and coarse grains show kink banding (Figure 3d). Some orthopyroxene grains occur as porphyroclasts, several mm across, with very thin clinopyroxene lamellae, if any, only at the core (Figure 3b,d). Chromian spinels show a light brownish color in the thin section (Figure 3c,e), of which tint is uniform throughout the samples, reflecting the lherzolitic lithology [41]. Some of them show vermicular shapes, intergrown with orthopyroxene and clinopyroxene (Figure 3e). Clinopyroxenes are smaller in size (less than a few mm across) than orthopyroxenes, and free from exsolution lamellae (Figure 3b,d). Phlogopite flakes are present in some of the xenoliths. They sometimes show ragged grain boundaries, enclosing small anhedral olivine and spinel grains. They rarely occur as veinlets cutting olivine (Figure 3f). These textures indicate the secondary origin of the Bankawa phlogopites.

The Bankawa peridotite xenoliths have been weathered and altered to various degrees (Figure 3) especially in the brecciated part (Figure 2). Some of them have been so severely altered that their olivines are totally replaced with clay minerals. Other minerals (pyroxenes and spinel) are almost intact from alteration even when olivines have been totally altered (Figure 3b).

4. Analytical Methods

4.1. Whole Rock

Whole rock major- and trace-element compositions were determined for three host basalt samples (B1, B2 and B3) with X-ray fluorescence spectrometry (XRF, Rigaku ZSX primus II) and laser ablation (193 nm ArF excimer: MicroLas GeoLas Q-plus)-inductively coupled plasma mass spectrometry (Agilent 7500 s) (LA-ICP-MS), respectively, at Kanazawa University, Japan [42]. Fused glass beads for the XRF analysis were prepared from flux ($Li_2B_4O_7$: 4.000 g) and rock powder (0.400 g) mixtures. In the LA-ICP-MS analysis, we prepared "flux-free fused glass" from samples by a direct fusion method (see [43]). The LA-ICP-MS analysis of the fused glass was performed with ablating of 100 μm diameter spots at 5 Hz repetition rate with energy density of 8 J·cm^{-2} per pulse. BCR-2G was used as an external calibration standard and its reference values were selected from the GeoReM database (see [44]). Data reduction was facilitated using ^{42}Ca as an internal standard, based on CaO content obtained from the XRF analysis, following a protocol essentially identical to that outlined by Longerich et al. [45]. Further technique and measurement quality were described in Kusano et al. [46] and Tamura et al. [43]. Whole rock compositions of the host rock are listed in Table 1.

4.2. Minerals

Six peridotite samples, which cover the whole petrographical variations, were carefully selected for detailed mineral chemistry analyses. Three of them (IZS-1, IZS-3 and IZS-6) are free from modal phlogopite while the other three (IZS-4, IZS-12 and IZS-13) contain it.

Major-element compositions of minerals in peridotite xenoliths were determined with an electron probe micro-analyzer (EPMA, JEOL JXA-8800R Superprobe) at Kanazawa University. The analysis was performed under an accelerating voltage of 20 kV and beam current of 20 nA, using a 3 μm diameter beam. Natural and synthetic minerals were used for standard materials, and a JEOL software (Tokyo, Japan) using ZAF corrections was used for data reduction. Representative major-element compositions of minerals are shown in Table 2. Trace-element compositions of clinopyroxene and orthopyroxene were determined by LA-ICP-MS at Kanazawa University. Each analysis was performed with ablating of 60 or 100 μm diameter spots at 6 Hz of repetition rate with energy density of 8 J·cm^{-2} per pulse. For the data reduction, the NIST (National Institute of Standards and Technology) 612 glass with selected reference values from Pearce et al. [47] was used as the primary calibration standard and ^{29}Si was used as internal

standards, based on SiO_2 contents obtained by microprobe analysis. The accuracy of measurements estimated from analyses of the NIST 614 glass is better than 5% (as relative standard deviation) for all elements. Trace-element compositions of clinopyroxene and orthopyroxene are listed in Tables 3 and 4, respectively.

Table 1. Whole rock compositions of host basalt from the Bankawa alkali basalt from the SW Japan arc.

Major Elements (wt %)	B1		B2		B3	
SiO_2	49.87		49.69		49.52	
TiO_2	1.40		1.54		1.43	
Al_2O_3	15.9		16.38		16	
Fe_2O_3	10.1		9.56		9.83	
MnO	0.17		0.16		0.17	
MgO	7.69		7.67		8.16	
CaO	9.2		9.27		9.4	
Na_2O	2.38		1.76		2.23	
K_2O	2.74		2.99		2.68	
P_2O_5	0.67		0.73		0.7	
Total	100.13		99.74		100.13	
LOI	0.06		0.07		0.06	
$Na_2O + K_2O$	5.12		4.75		4.91	
CIPW Norm						
Or	16		18		16	
Ab	20		15		19	
An	25		28		26	
Di	14		11		13	
Hy	5		14		6	
Ol	13		7		13	
Mt	4		4		4	
Il	3		3		3	
Ap	2		2		2	
Trace Elements (μg/g)	**AVE**	**SD**	**AVE**	**SD**	**AVE**	**SD**
Li	12.7	0.1	15.9	0.2	13.6	0.6
Sc	25.1	0.2	26.3	0.2	25.5	0.3
Ti	8529	72	9539	57	8996	281
V	214.3	0.3	237.3	0.6	212.7	4.4
Cr	253	48	290	16	136	48
Co	34.3	0.5	37.8	0.1	36.4	0.3
Ni	139	5	147	2	152	3
Rb	80.6	1.7	96.8	1.2	81.3	7.6
Sr	896	6	1560	7	1316	12
Y	24.3	0.24	25.23	0.38	24.86	0.28
Zr	180.6	1.1	190.6	2.3	191.7	4.1
Nb	60.29	0.42	69.10	0.51	66.21	2.03
Cs	2.6	0.18	3.3	0.03	3.3	0.62
Ba	619.1	4.7	936.8	6.5	654.3	21.9
La	44.44	0.35	48.24	0.24	46.90	0.77
Ce	84.6	0.57	93.93	0.89	90.61	1.79
Pr	9.20	0.09	10.04	0.09	9.74	0.16
Nd	35.23	0.53	37.95	0.34	37.01	0.5
Sm	6.48	0.02	6.84	0.04	6.72	0.07
Eu	1.94	0.02	2.08	0.04	2.00	0.02
Gd	5.53	0.09	5.79	0.07	5.73	0.08
Tb	0.78	0.01	0.81	0.01	0.79	0.01
Dy	4.57	0.07	4.78	0.05	4.66	0.05
Ho	0.88	0.01	0.90	0.02	0.88	0.01
Er	2.47	0.03	2.57	0.03	2.50	0.04
Tm	0.35	0.01	0.36	0.01	0.34	0.01
Yb	2.31	0.03	2.41	0.03	2.31	0.03
Lu	0.34	0.01	0.35	0.01	0.35	0.01
Hf	4.11	0.07	4.29	0.04	4.20	0.12
Ta	3.37	0.06	3.72	0.04	3.63	0.09
Th	8.38	0.12	8.77	0.08	8.57	0.23

Note: Loss on ignition (LOI) was determined before and after ignition at 900 °C for four hours; CIPW Norm calculated based on $Fe^{3+}/Fe^{2+} = 0.15$.; AVE, averages of 3 spot analyses using fused glass method; SD, 1 sigma standard deviation.

Table 2. Representative major-element compositions of minerals in peridotite xenoliths from Bankawa, the SW Japan arc.

	IZS-1				IZS-3				IZS-4				
	Lherzolite				Lherzolite				Phl-lherzolite				
	Olivine	Cpx	Opx	Spinel	Olivine	Cpx	Opx	Spinel	Olivine	Cpx	Opx	Spinel	Phl
(wt %)	#113	#106	#109	#110	#5	#82	#8	#7	#115	#124	#126	#125	#117
SiO_2	41.07	52.75	55.92		40.68	54.18	55.87		40.75	52.91	56.14		38.40
TiO_2		0.02		0.02		0.07	0.03	0.03		0.13	0.02	0.07	1.48
Al_2O_3	0.01	3.75	3.44	41.94	0.03	3.97	3.28	40.30	0.01	3.75	3.23	40.58	16.86
Cr_2O_3		0.78	0.52	24.97		0.98	0.59	26.70	0.01	0.84	0.51	25.63	1.46
FeO *	9.16	2.75	5.91	14.02	9.04	2.77	5.83	14.07	9.13	2.73	5.94	14.45	3.90
MnO	0.11	0.10	0.12	0.16	0.13	0.08	0.14	0.16	0.14	0.08	0.15	0.17	0.02
MgO	50.04	17.59	33.66	18.54	50.11	17.10	33.62	18.22	50.14	17.33	33.67	18.21	22.13
CaO	0.08	22.22	1.01		0.06	21.57	0.91		0.06	22.12	0.90		0.02
Na_2O		0.08				0.83	0.05			0.21	0.01		0.10
K_2O		0.01	0.01	0.01				0.01					9.98
NiO	0.38	0.06	0.09	0.29	0.35	0.06	0.09	0.26	0.38	0.06	0.10	0.24	0.18
Total	100.86	100.11	100.67	99.97	100.40	101.59	100.41	99.76	100.63	100.17	100.66	99.39	94.51
Mg#	0.907	0.919	0.910	0.763	0.908	0.917	0.911	0.757	0.907	0.919	0.910	0.758	0.910
Cr#				0.285				0.308				0.298	
Y_{Fe}				0.044				0.043				0.048	
T1 (°C)	1039				1011				1027				
T2 (°C)	1129				1107				1119				

	IZS-6			IZS-12					IZS-13				
	Lherzolite			Phl-lherzolite					Phl-lherzolite				
	Cpx	Opx	Spinel	Olivine	Cpx	Opx	Spinel	Phl	Olivine	Cpx	Opx	Spinel	Phl
(wt %)	#183	185	#110	#203	#242	#204	#239	#220	#167	#129	#159	#164	#130
SiO_2	53.47	56.55		40.79	52.39	55.68		37.40	40.61	52.62	55.52		39.00
TiO_2	0.08	0.03	0.02		0.70	0.14	0.51	6.82		0.48	0.16	0.39	3.54
Al_2O_3	3.78	3.57	41.94		5.13	3.23	40.33	15.93	0.02	4.88	3.52	40.29	16.86
Cr_2O_3	0.81	0.56	24.97	0.01	1.10	0.48	25.18	1.36		0.84	0.53	24.99	1.06
FeO *	2.76	6.01	14.02	12.96	3.10	8.25	16.68	4.16	9.81	2.98	6.59	15.05	4.50
MnO	0.09	0.15	0.16	0.25	0.10	0.23	0.16	0.02	0.17	0.12	0.14	0.18	0.02
MgO	17.87	33.97	18.54	47.09	16.29	31.62	17.93	19.55	49.05	16.32	32.88	18.20	21.27

Table 2. *Cont.*

	IZS-6			IZS-12					IZS-13				
	Lherzolite			Phl-lherzolite					Phl-lherzolite				
	Cpx	Opx	Spinel	Olivine	Cpx	Opx	Spinel	Phl	Olivine	Cpx	Opx	Spinel	Phl
(wt %)	#183	185	#110	#203	#242	#204	#239	#220	#167	#129	#159	#164	#130
CaO	22.32	1.11		0.08	21.12	1.00		0.02	0.08	20.58	0.93		0.01
Na_2O	0.10				0.86	0.04		0.54		0.86	0.03		0.86
K_2O				0.01				9.10		0.01	0.01		8.95
NiO	0.05	0.08	0.29	0.30	0.06	0.05	0.28	0.19	0.35	0.04	0.09	0.28	0.20
Total	101.32	102.02	99.97	101.49	100.83	100.72	101.12	95.08	100.10	99.72	100.40	99.44	96.26
Mg#	0.920	0.910	0.763	0.866	0.904	0.872	0.736	0.893	0.899	0.907	0.899	0.756	0.894
Cr#			0.285				0.295					0.29	
Y_{Fe}			0.044				0.061					0.054	
T1 (°C)	1053				993					1028			
T2 (°C)	1140				1061					1111			

* Total iron as FeO; Mg# = Mg/(Mg + Fe^{2+}), Cr# = Cr/(Cr + Al), Fe^{3+}# = Fe^{3+}/(Cr + Al + Fe^{3+}); Fe^{2+} and Fe^{3+} of spinel were calcualted based on stoichiometry; Y_{Fe} = Fe^{3+}/(Cr + Al + Fe^{3+}); T1 and T2 are calculated temperatures from the geothermometry by Wells [48] and Wood and Banno [49], respectively; Phl, phlogopite.

Table 3. Trace-element compositions of clinopyroxene in peridotite xenoliths from Bankawa, the SW Japan arc.

	IZS-1				IZS-3			IZS-4			
	Lherzolite				Lherzolite			Phl-lherzolite			
(µg/g)	#101	#102	#103	#113 **	#201	#202	#203	#301	#302	#303	#313 **
Sc	50	50	50	52	65	71	73	50	52	52	51
Ti	221	210	215	229	293	435	396	438	500	594	532
V	269	256	264	263	287	301	308	237	239	253	242
Cr	5963	4687	5215	5679	5882	7020	7064	5469	5269	7179	8535
Co	28	28	28	27	25	24	24	26	27	26	35
Ni	451	446	449	450	392	386	394	431	441	437	512
Sr	0.54	0.62	1.24	0.43	19.92	51.55	47.61	26.96	29.41	32.46	31.69
Y	3.37	3.21	3.34	3.52	3.60	5.22	5.02	4.26	4.55	5.04	4.78
Zr	0.05	0.05	0.07	0.05	0.32	4.03	2.80	5.96	7.11	9.94	9.75
Nb	0.24	0.20	0.23	0.23	0.57	0.77	0.75	0.59	0.68	0.80	0.71

Table 3. *Cont.*

(µg/g)	IZS-1				IZS-3			IZS-4			
	Lherzolite				Lherzolite			Phl-lherzolite			
	#101	#102	#103	#113 **	#201	#202	#203	#301	#302	#303	#313 **
La	0.111	0.100	0.147	0.086	2.532	4.234	4.054	2.172	2.375	2.554	2.325
Ce	0.091	0.104	0.172	0.081	4.753	10.643	9.751	5.639	6.117	6.822	6.393
Pr	0.004	0.005	0.010	0.003	0.351	1.154	1.000	0.621	0.694	0.807	0.798
Nd			0.023	0.008	0.889	4.285	3.573	2.444	2.746	3.363	3.486
Sm		0.030	0.030	0.032	0.122	0.690	0.542	0.458	0.488	0.642	0.653
Eu	0.021	0.018	0.018	0.017	0.044	0.234	0.178	0.133	0.154	0.192	0.197
Gd	0.155	0.142	0.148	0.173	0.192	0.639	0.533	0.457	0.519	0.650	0.604
Tb	0.047	0.050	0.049	0.054	0.052	0.117	0.095	0.083	0.090	0.113	0.104
Dy	0.493	0.485	0.499	0.544	0.519	0.874	0.812	0.707	0.770	0.882	0.835
Ho	0.130	0.130	0.137	0.145	0.136	0.209	0.191	0.163	0.174	0.207	0.191
Er	0.446	0.407	0.467	0.490	0.480	0.661	0.649	0.545	0.565	0.652	0.586
Tm	0.067	0.067	0.070	0.077	0.078	0.114	0.098	0.086	0.090	0.100	0.088
Yb	0.493	0.489	0.502	0.540	0.590	0.760	0.766	0.591	0.639	0.705	0.624
Lu	0.072	0.069	0.073	0.081	0.085	0.117	0.120	0.083	0.089	0.098	0.093
Hf								0.15	0.27	0.40	0.22
Ta					0.04	0.08	0.07	0.06	0.08	0.09	0.08
Th	0.04	0.04	0.05	0.04	0.11	0.15	0.14	0.12	0.14	0.15	0.14
U					0.02	0.03	0.03	0.03	0.04	0.04	0.03

(µg/g)	IZS-6			IZS-12			IZS-13			DL60 *
	Lherzolite			Phl-lherzolite			Phl-lherzolite			
	#301_06	#302	#303	#201_12	#202	#203	#101_13	#102	#103	
Sc	50	49	49	58	75	70	59	59	57	0.1
Ti	353	344	340	2053	3387	3358	2765	2667	2710	0.5
V	243	238	237	280	343	294	238	250	235	0.1
Cr	6844	6993	6214	8392	8221	6573	6708	7754	6727	3
Co	28	29	28	25	24	24	25	25	25	0.0
Ni	447	466	453	346	394	393	380	384	375	1
Sr	0.04	0.04	0.06	103.32	94.26	86.66	165.90	162.52	159.85	0.01
Y	4.16	4.00	3.88	13.31	11.33	10.55	14.66	15.11	14.57	0.008
Zr	0.06	0.06	0.05	27.70	24.25	20.10	36.45	42.42	38.85	0.02
Nb	0.13	0.13	0.12	0.34	0.31	0.77	0.72	0.71	0.78	0.01

Table 3. *Cont.*

(µg/g)	IZS-6			IZS-12			IZS-13			DL60 *
	Lherzolite			Phl-lherzolite			Phl-lherzolite			
	#301_06	#302	#303	#201_12	#202	#203	#101_13	#102	#103	
La	0.015	0.016	0.024	5.040	5.920	4.268	8.428	8.725	8.453	0.009
Ce	0.010	0.014	0.021	19.634	19.572	14.777	28.043	30.145	28.044	0.004
Pr				2.984	2.723	2.130	3.807	4.147	3.945	0.004
Nd				14.468	13.089	10.835	17.310	18.754	18.110	0.03
Sm	0.040	0.034	0.034	3.552	3.088	2.789	3.933	4.235	4.029	0.03
Eu	0.028	0.030	0.024	1.154	1.011	0.878	1.304	1.404	1.327	0.009
Gd	0.239	0.198	0.200	3.133	2.813	2.603	3.283	3.662	3.523	0.05
Tb	0.060	0.065	0.060	0.433	0.409	0.378	0.472	0.484	0.494	0.009
Dy	0.625	0.626	0.575	2.869	2.489	2.300	3.034	3.201	3.106	0.02
Ho	0.165	0.158	0.154	0.515	0.493	0.439	0.588	0.615	0.595	0.01
Er	0.537	0.532	0.488	1.452	1.239	1.162	1.568	1.643	1.619	0.02
Tm	0.083	0.077	0.082	0.206	0.176	0.151	0.218	0.218	0.229	0.01
Yb	0.592	0.596	0.564	1.462	1.106	1.014	1.528	1.571	1.599	0.03
Lu	0.082	0.086	0.083	0.189	0.142	0.130	0.210	0.217	0.212	0.01
Hf				0.53	0.79	0.96	1.25	1.34	1.34	0.07
Ta				0.05	0.05	0.06	0.16	0.14	0.14	0.009
Th				0.11	0.45	0.19	0.23	0.31	0.26	0.02
U				0.02	0.11	0.05	0.05	0.07	0.05	0.01

Blank, data below the detection limit; * Detection limit of 60 µm laser-ablation spot size; ** 100 µm spot size was used (for detection limit, see Table Table 4); Phl, phlogopite.

Table 4. Trace-element compositions of orthopyroxene in peridotite xenoliths from Bankawa, the SW Japan arc.

	IZS-1			IZS-3			IZS-4		ISZ-6			ISZ-12		ISZ-13			DL100 *
	Lherzolite			Lherzolite			Phl-lherzolite		Lherzolite			Phl-lherzolite		Phl-lherzolite			
(µg/g)	#111	#112	#114	#211	#212	#213	#311	#312	#311	#312	#313	#111	#114	#111	#112	#113	
Sc	27	27	29	21	22	22	24	25	27	26	25	19	17	16	16	15	0.03
Ti	91	90	97	106	139	122	210	196	144	142	139	668	693	877	833	658	0.09
V	149	146	160	118	118	132	124	133	134	133	130	124	105	87	85	83	0.02
Cr	3905	3673	4460	3836	3840	4148	3804	4082	4456	4844	4482	4423	4140	3775	3510	3245	0.5
Co	64	63	64	59	60	60	63	62	63	63	61	61	63	62	62	62	0.01
Ni	836	834	838	761	767	765	805	801	832	837	802	674	686	760	765	747	0.2
Sr				0.032	0.087	0.163	0.053	0.068	0.045	0.061	0.003	0.776	0.530	0.351	0.379	0.400	0.003
Y	0.413	0.417	0.453	0.301	0.443	0.373	0.517	0.530	0.510	0.496	0.462	1.188	1.284	1.432	1.467	1.453	0.001
Zr	0.032	0.028	0.035	0.046	0.283	0.042	0.931	0.907	0.035	0.033	0.039	1.522	1.982	3.630	3.768	3.277	0.005
Nb	0.043	0.048	0.042	0.057	0.062	0.082	0.095	0.093	0.053	0.052	0.048	0.056	0.049	0.067	0.064	0.063	0.001
La				0.004	0.007	0.030	0.006	0.006				0.034	0.022	0.018	0.020	0.020	0.002
Ce				0.014	0.031	0.055	0.026	0.026				0.151	0.095	0.121	0.119	0.116	0.001
Pr				0.002	0.005	0.004	0.004	0.005				0.027	0.020	0.024	0.024	0.021	0.001
Nd							0.021	0.024				0.155	0.126	0.157	0.152	0.143	0.004
Sm					0.007		0.009					0.063	0.053	0.071	0.064	0.066	0.009
Eu					0.004		0.004	0.002				0.025	0.024	0.030	0.031	0.028	0.001
Gd					0.017		0.019	0.018				0.091	0.101	0.115	0.110	0.105	0.01
Tb	0.002	0.003	0.003		0.005	0.003	0.005	0.004	0.005	0.003	0.003	0.020	0.022	0.023	0.025	0.024	0.002
Dy	0.043	0.043	0.044	0.030	0.046	0.038	0.055	0.060	0.054	0.049	0.049	0.167	0.190	0.202	0.205	0.199	0.005
Ho	0.015	0.015	0.016	0.013	0.016	0.013	0.017	0.018	0.018	0.018	0.015	0.038	0.045	0.053	0.051	0.052	0.003
Er	0.065	0.071	0.072	0.051	0.067	0.058	0.078	0.083	0.083	0.078	0.078	0.152	0.167	0.196	0.184	0.190	0.006
Tm	0.015	0.015	0.016	0.012	0.015	0.014	0.016	0.017	0.015	0.019	0.015	0.029	0.032	0.037	0.038	0.038	0.003
Yb	0.144	0.142	0.158	0.116	0.147	0.124	0.156	0.153	0.163	0.156	0.146	0.267	0.282	0.324	0.306	0.308	0.007
Lu	0.027	0.025	0.029	0.022	0.027	0.025	0.030	0.030	0.029	0.029	0.027	0.044	0.050	0.057	0.056	0.054	0.002

Blank, data below the dection limit; * 100 µm spot size was used; Phl, phlogopite.

5. Chemistry of the Host Rock

The host rock contains about 50 wt % SiO_2, 16 wt % Al_2O_3 and 5 wt % total alkalis ($Na_2O + K_2O$). TiO_2 and P_2O_5 contents are 1.4–1.5 wt % and 0.7 wt %, respectively. It is relatively silica-rich alkali basalt, containing normative hypersthene and olivine (Table 1). The Bankawa alkali basalt is within the field of Cenozoic basalts in and around the SW Japan arc in the SiO_2-alkalis space (Figure 4).
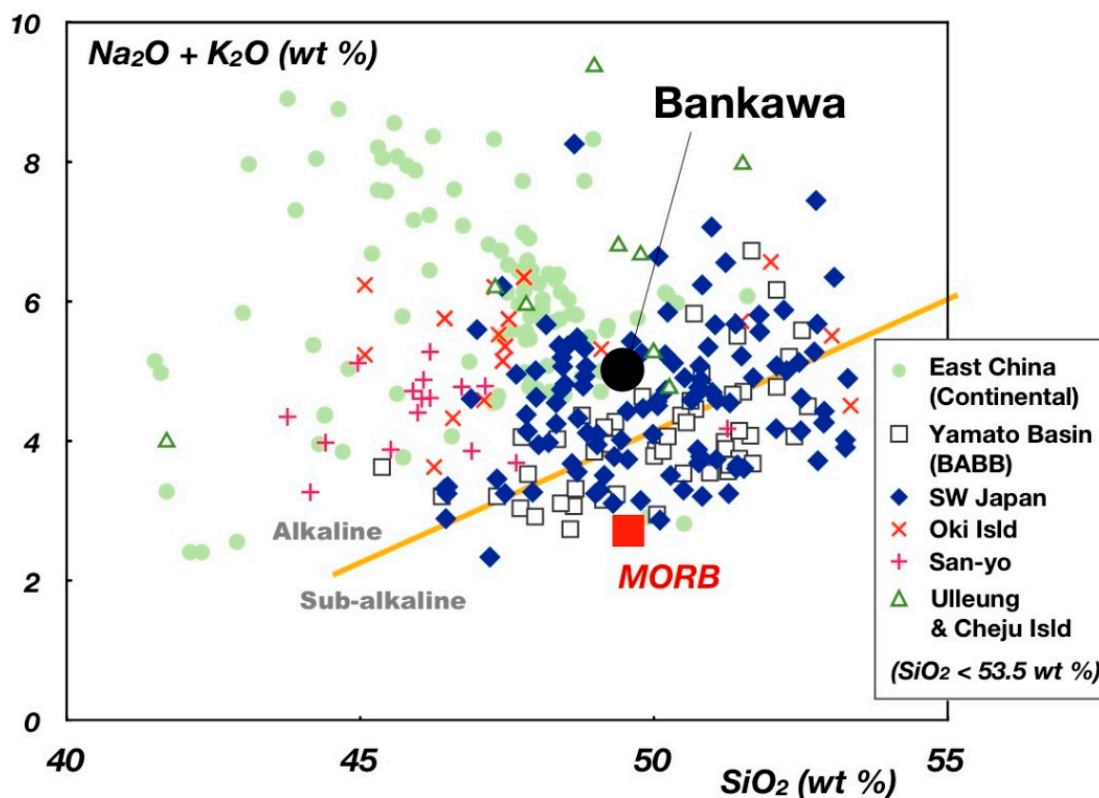
Figure 4. SiO_2 vs. total alkali ($Na_2O + K_2O$) of the host alkali basalt. The solid yellow line is the boundary between alkali- and subalkali-basalts of Miyashiro [50]. Reference data are selected alkali basalts ($SiO_2 < 53.5$ wt %) from SW Japan, east China, and back-arc basin basalts from Yamato basin, the Sea of Japan. Data source; SW Japan, Oki Island and San-yo [51–56]: Ulleung and Cheju Islands [51,52,57]: East China [51,58–61]: Yamato Basin (ODP Leg 127/128, Sea of Japan) [62,63].

The Bankawa alkali basalt hosting the xenoliths is very similar in trace-element (primitive mantle normalized) and REE (chondrite-normalized) patterns to the Cenozoic alkali basalts from the SW Japan arc, some of which contain mantle peridotite xenoliths [64] (Figure 5). The patterns are simple, being almost monotonously declining from more incompatible element to less incompatible one (Figure 5), although it shows slight troughs at Zr, Hf and Ti.
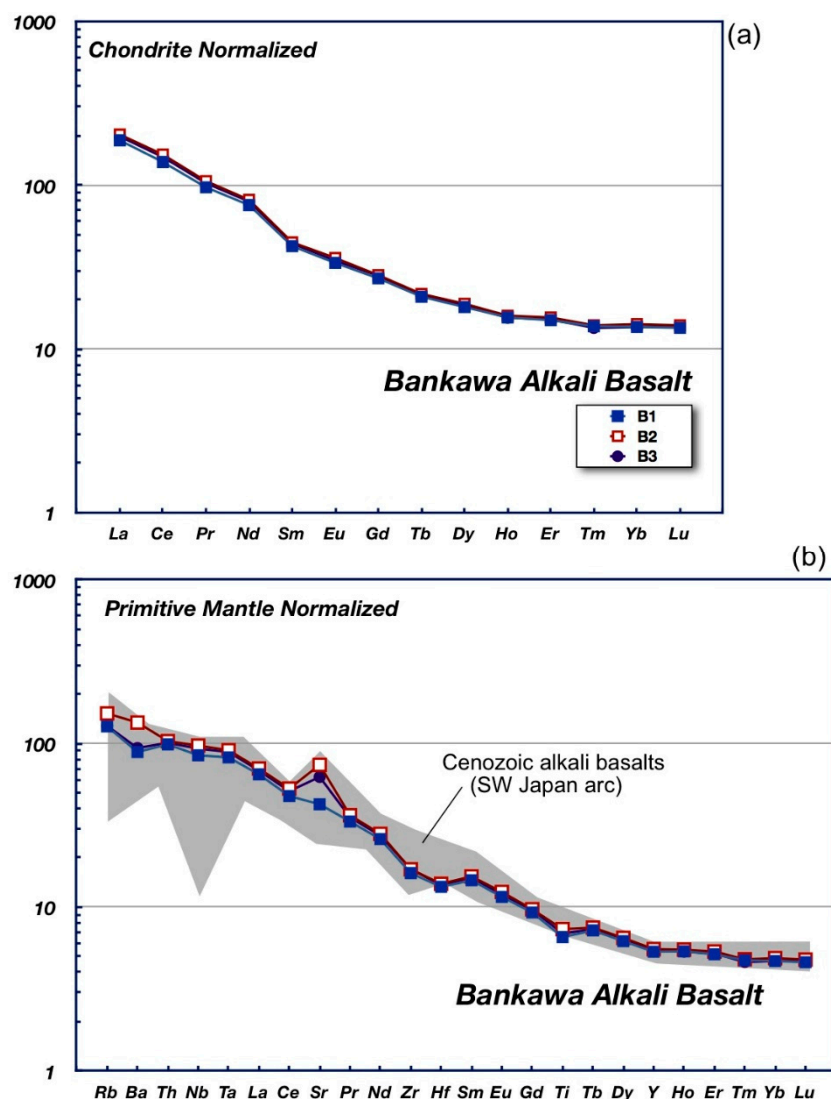
Figure 5. Trace-element characteristics of the Bankawa host alkali basalt. (**a**) chondrite-normalized REE pattern; (**b**) primitive mantle normalized trace-element pattern. Three samples (B1, B2 and B3) were analyzed. Range of Cenozoic alkali basalts from the SW Japan arc [54] are shown for comparison. Normalized values are from Sun and McDonough [65].

6. Mineral Chemistry

6.1. Major Elements

6.1.1. Host Alkali Basalt

Olivine phenocrysts are magnesian and show Fo_{90-82} ($Fo = 100Mg/[Mg + Fe^{2+}]$) in composition. Their NiO content is 0.1–0.2 wt % (Figure 6). Chromian spinel inclusions in olivine show a very limited range of composition. The Cr# (=Cr/(Cr + Al) atomic ratio) ranges from 0.3 to 0.4, and the Y_{Fe} ($=Fe^{3+}/(Cr + Al + Fe^{3+})$ atomic ratio) is lower than 0.1 (Figure 7). The chromian spinel is relatively low in TiO_2 (<1 wt %), and plotted around the boundary between intraplate and arc magmas in the TiO_2-Y_{Fe} space [66]. The Bankawa alkali basalt shows a very primitive character in terms of the Fo (olivine)-Cr# (spinel) relationship [41,67,68] (Figure 8). Some of the olivine–spinel pairs in the host rock are plotted in or near the olivine–spinel mantle array, a residual spinel peridotite field (Figure 8) [41,67].
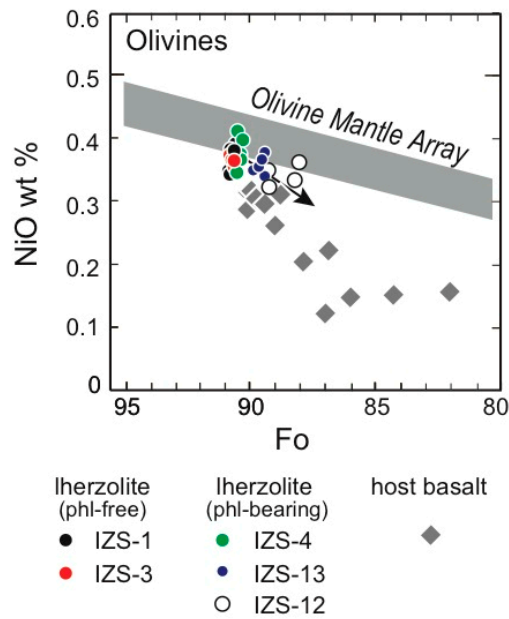
Figure 6. Fo vs. NiO relations of olivine. Olivine-Mantle Array (mantle peridotite range) is after Takahashi [69]. Note that the olivines in the phlogopite-bearing lherzolite are slightly lower in Fo and NiO content. Note that olivine has been altered in one of our samples (IZS-06). The arrow indicates a possible metasomatic trend.
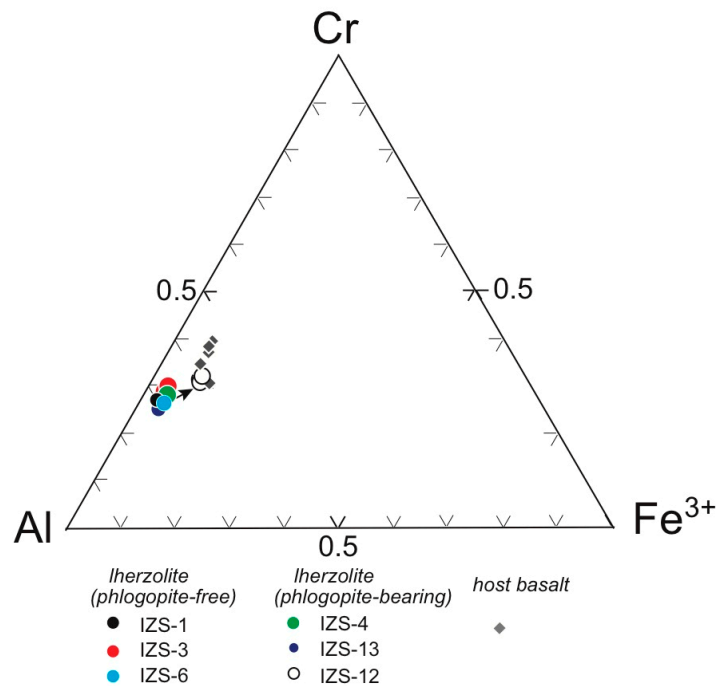
Figure 7. Trivalent cation relations of chromian spinel. Note that the chromian spinel in the lherzolite containing phlogopite veinlets (Figure 3f) is similar to that in the host basalt (inclusions in olivine phenocrysts). The arrow indicates a possible metasomatic trend.

6.1.2. Peridotites

Chemical properties of minerals apparently vary in response to the extent of metasomatic addition of phlogopite (see Section 8.2. below for discussion). Phlogopite-free lherzolites show very uniform and relatively refractory mineral chemistry; their olivines show the Fo content slightly lower than 91 and contain about 0.4 wt % NiO (Figure 6). The Cr# and Y_{Fe} of their chromian spinel are around 0.3

and lower than 0.05, respectively (Figures 7 and 8). The Mg# is about 0.91 and 0.92 for orthopyroxenes and clinopyroxenes, respectively. Clinopyroxenes are chromian diopside containing 0.8 to 1 wt % Cr_2O_3, and are characterized by low Na_2O (<0.1 wt %) and TiO_2 (0.1 wt %) contents (Table 2). The Bankawa phlogopite-free lherzolite is plotted in the olivine mantle array [66] (Figure 6) and in the olivine–spinel mantle array [41] (Figure 8). It is characterized as a slightly refractory lherzolite in terms of the olivine–spinel mantle array (Figure 8), which is consistent with the modal composition (i.e., clinopyroxene-poor lherzolite). The Bankawa phlogopite-free lherzolite is similar to abyssal peridotite in terms of Na_2O content of clinopyroxene and Cr# of associated chromian spinel [4,70] (Figure 9).
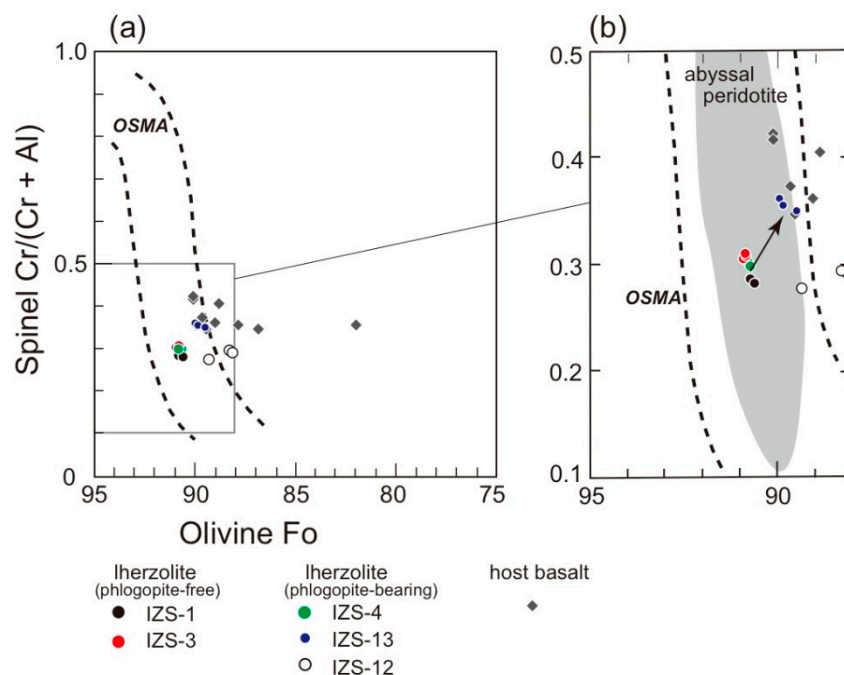
Figure 8. Fo (olivine)-Cr# (chromian spinel) relations. The main part of (**a**) is enlarged as (**b**). The field between the broken lines is the olivine–spinel mantle array (OSMA) [41]. The field of abyssal peridotites is after Arai [41]. Note that olivine has been altered in one of our samples (IZS-06). The arrow indicates a possible metasomatic trend. Note that the phlogopite-free lherzolite is very confined on the Fo(olivine)-Cr# (spinel) space.

With an increase in the amount of secondary phlogopites, all the primary minerals seem to get less refractory in chemistry. The Fo content of olivine is lowered even to 87, showing a very weak positive correlation with the NiO content, in the phlogopite-bearing lherzolites (Figure 6). Pyroxenes are also slightly lower in Mg# in the phlogopite-bearing lherzolites than in the phlogopite-free ones. The Na_2O (up to 0.9 wt %) and TiO_2 (0.5 wt %) contents of clinopyroxene are remarkably high in the phlogopite-bearing lherzolites (Table 2). Sample IZS-3 is exceptional; it is free of modal phlogopite, but its clinopyroxene is high in Na_2O (~ 0.8 wt %). Chromian spinel is also enriched with Ti (up to 0.5 wt % TiO_2) with addition of the secondary phologopite (Table 2). The Y_{Fe} of spinel is also slightly higher in a phlogopite-bearing lherzolite (IZS-12) (Figure 7). The Cr# of spinel is remarkably high (up to 0.36) in a phlogopite-bearing sample (IZS-13) (Figure 8). The Cr# and Y_{Fe} of chromian spinel seem to approach those of spinel in the host alkali basalt (Figure 7).
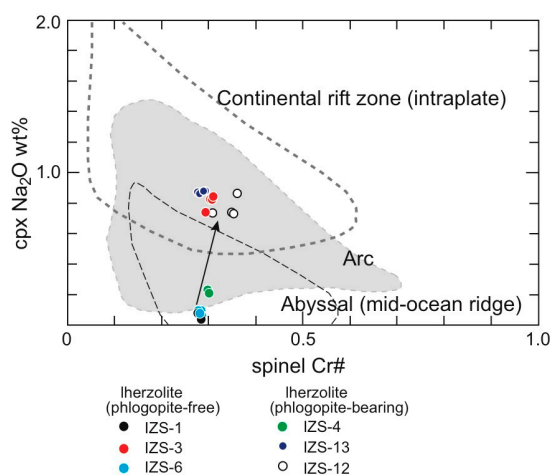
Figure 9. Relationship between Na_2O of clinopyroxene and Cr# of chromian spinel in the Bankawa lherzolites. Note that the unmetasomatized (phlogopite-free) lherzolite contains Na-poor clinopyroxene and is similar to the abyssal peridotite. The discrimination fields are after Arai [41,70]. The arrow indicates a possible metasomatic trend.

Phlogopites are variable in TiO_2 content (1 to 11 wt %) and in Na/(K + Na) ratio (0.01 to >0.1 in atom) (Table 2; Figure 10a), as observed in metasomatic phlogopites in peridotites [71,72]. They are totally within the field for the secondary phlogopites in continental rift-zone peridotites (Figure 10a). The Bankawa phlogopite is high in eastonite component (Si = ca. 5.5 on O = 22), being within the field of secondary phlogopites in spinel peridotite [73] (Figure 10b), consistent with the presence of spinel.
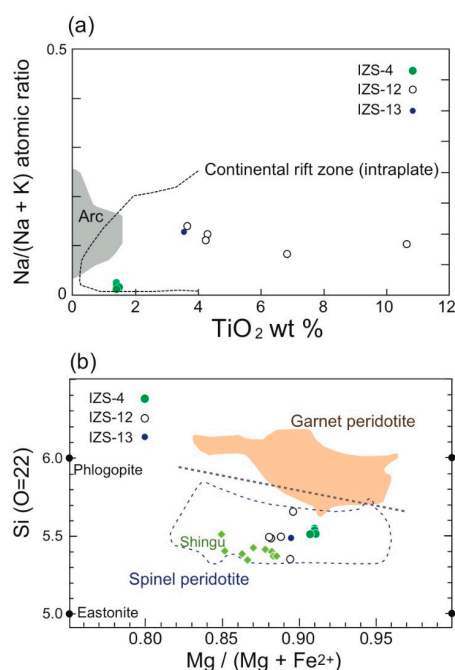
Figure 10. Chemical characteristics of secondary phologopites. (**a**) relationship between Na/(Na + K) ratio and TiO_2 content. Fields for arc peridotite (peridotite xenoliths in arc magmas) and intraplate peridotites (peridotite xenoliths in intraplate magmas) were determined from the literature data [18,19,71,74–80]. Note that abyssal peridotites only rarely contain phlogopites [81]; (**b**) relationship between Si content (number of Si on O=22) and Mg/(Mg + Fe^{2+}) atomic ratio. Fields for garnet peridotite and spinel peridotite are after Arai [73]. Phlogopites from metasomatized peridotite xenolith from Shingu [82] (Figure 1) are plotted for comparison.

6.2. Trace Elements in Pyroxenes

The REE pattern of clinopyroxene normalized to chondrite changes apparently depends on the degree of phlogopite addition (Figure 11a). Clinopyroxene shows a spoon-like pattern, simply declining from Lu to Nd and slightly enriched in LREE (light REE), in two phlogopite-free samples (IZS-6, IZS-1). Two other samples (IZS-3, IZS-4) contain clinopyroxenes that show concave upward REE patterns, where enrichment in LREE is remarkable (Figure 11a). One of the samples (ISZ-4) contains phlogopite, but clinopyroxenes in the other (IZS-3), which is free of modal phlogopite, are as high in Na_2O (0.8 wt %) as those in phlogopite-bearing peridotites (Figure 9; Table 2). Clinopyroxenes in the other two phlogopite-bearing samples (IZS-12, IZS-13) exhibit a monotonous LREE-enriching pattern (Figure 11a). The REE abundances successively increase with a change of the pattern from the spoon-like one to the LREE-enriching one through the concave upward one with MREE (middle REE) depletion (Figure 11a). Clinopyroxenes in all the Bankawa lherzolites show depletions at Ti and Zr in chondrite-normalized trace-element patterns (Figure 11b) as frequently observed in mantle-derived peridotites including abyssal peridotites [83–85]. They show prominent negative anomalies at Sr in the phlogopite-bearing samples (Figure 11b), being reciprocal to the frequent positive Sr anomaly in the host alkali basalt (Figure 5b).
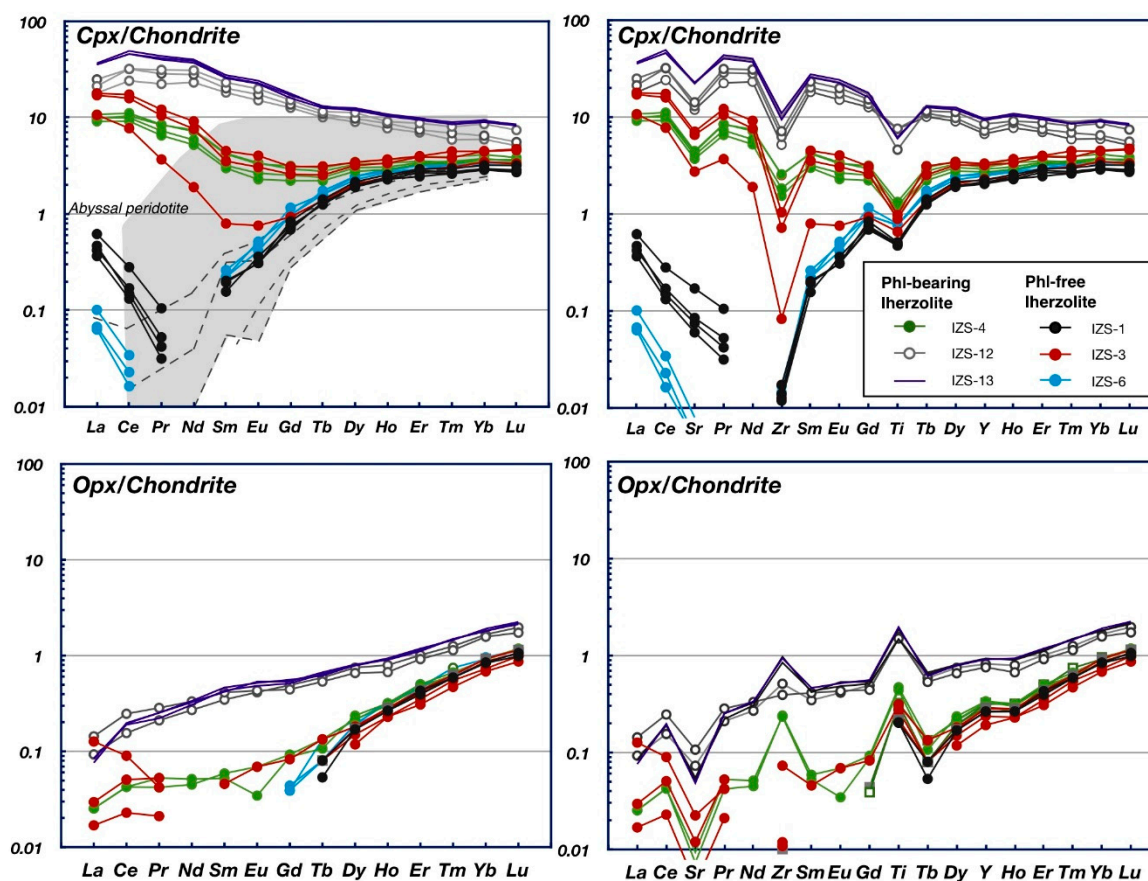
Figure 11. Chondrite-normalized REE and trace-element patterns of pyroxenes in the Bankawa lherzolite. (**a**,**b**) Clinopyroxene. (**c**,**d**) Orthopyroxene. Normalization values from Sun and McDonough [65]. Abyssal peridotite field (grey in (**a**)) is compiled from Johnson et al. [86], Johnson and Dick [87] and Hellebrand et al. [88]. Some examples of the clinopyroxne pattern in depleted abyssal peridotite are shown by broken lines for comparison.

Orthopyroxenes show a monotonous decrease from HREE toward LREE in chondrite-normalized patterns for all samples examined (Figure 11c). MREE were not detected in orthopyroxenes from the phlogopite-free samples (Figure 11c). The orthopyroxene pattern shows an almost gradual

decrease from HREE to LREE and higher levels of REE in the phlogopite-bearing lherzolite than in the phlogopite-free one (Figure 11c). Orthopyroxenes show positive anomalies at Zr and Ti (Figure 11b), which are complementary to the negative spike at these elements in the clinopyroxene patterns (Figure 11d) [89]. They exhibit negative Sr anomaly (Figure 11d), which is frequently observed in abyssal peridotites [85].

7. Geothermobarometry

No reliable barometers have been developed for spinel peridotites. The Bankawa lherzolites contain neither plagioclase nor garnet, and are most probably derived from the spinel-lherzolite stability field as peridotite xenoliths from the Japan arcs and other arc areas [2,4].

The two-pyroxene thermometer [48,49] gave a very limited range of equilibrium temperature (993 to 1053 °C), which is included in the range of low-temperature peridotite xenoliths from the SW Japan arc [2,4,6] (Figure 12a).
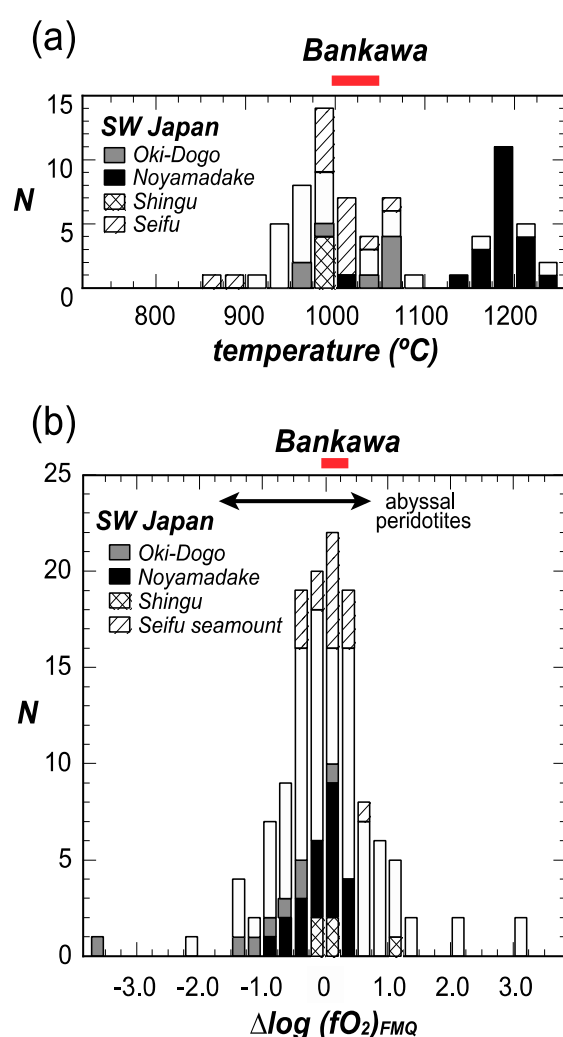
Figure 12. Ranges of equilibrium temperature and oxygen fugacity of the Bankawa lherzolite in comparison with peridotite xenoliths from the SW Japan arc. Histograms are from Arai and Ishimaru [4,6]. Temperatures were calculated after Wells [48]. Δlog(fO$_2$)$_{FWQ}$ is calculated oxygen fugacity relative to the fayalite–magnetite–quartz buffer assuming a pressure of 1.5 GPa [90].

The olivine–orthopyroxene–spinel oxygen barometer of Ballhaus et al. [90] yields a very limited range, -0.08 to 0.32, of Δlog(fO$_2$)$_{FMQ}$ (= a log unit difference in oxygen fugacity from the fayalite-magnetite-quartz buffer) assuming a pressure of 1.5 GPa (within the spinel lherzolite field).

The range is within that of abyssal peridotite or that of the peridotite xenoliths from the SW Japan arc [4] (Figure 12b).

8. Discussion

8.1. Importance of the Bankawa Xenolith Suite; Pristine Nature of the Peridotite

The Bankawa area is located in a quite unique place in the Japan arcs (Figure 1); it is on the Quaternary mantle wedge of the Southwest Japan arc and remote from the Japan Sea side of the Honshu and Kyushu islands that have a large number of mantle xenolith localities [1,2,4,16] (Figure 1). The sedimentary basin for the Izumi Group is one of strike-slip depressions along the Median Tectonic Line (Figure 1). The tectonism that formed this kind of basin possibly affected only a crustal part above the tip of the mantle wedge [91]. It is expected that the mantle part beneath the Izumi sedimentary basin was not tectonically disturbed and has not been serpentinized. The Pacific side of the SW Japan arc was impacted by magmatism in the Miocene [27,31] triggered by subduction of the Shikoku Basin, which was/is part of the Philippine Sea plate (Figure 1). The Shikoku Basin was formed as a backarc basin of the Izu–Bonin–Mariana arc, and young and still hot at that time. The Miocene magmatism includes high-Mg andesite (sanukitoid) eruption around the Setouchi belt [25,92] and intrusion of high-level granitoids [93] (Figure 1). The Bankawa area is just between the Setouchi high-Mg andesite belt to the north and the outer granitoid belt to the south (Figure 1). The Bankawa peridotite (lherzolite) is derived from the upper mantle that has not been disturbed by the magmatism and tectonism younger than the Paleogene. The Ryoke metamorphic belt (of low P/T type) possibly underlays the Izumi basin [94], and the Bankawa lherzolite may be representative of the upper mantle beneath the low P/T type part of the paired metamorphic belts.

We note that the Bankawa xenolith suite is free from any discrete Group II rocks (black clinopyroxene-bearing coarse-grained peridotites and pyroxenites) [40]. The mantle peridotite xenoliths associated with Group II rocks were severely metasomatized in both petrography and chemistry in the SW Japan arc [1]. Arai et al. [1] suggested that mantle peridotite xenoliths captured by alkali basalt, especially by that from monogenetic volcano clusters, were inevitably modified by preceding magmas cogenetic with their host basalt. We therefore expect limited metasomatic effects on the Bankawa lherzolite xenoliths from the magma cogenetic with the host alkali basalt because the Bankawa dike is solitary and the xenolith suite is free of Group II rocks [1]. This is in contrast to the xenolith suite of Shingu, which is located at Shikoku Island and the most Pacific-ward xenolith locality in the SW Japan arc (Figure 1) [82,95]. The Shingu xenolith suite includes a large amount of Group II rocks and related megacrysts, and was intensely metasomatized by a deep-seated alkali basalt magma related with the host magma [82].

8.2. Origin of the Mantle Metasomatism and the Host Alkali Basalt

The Bankawa alkali basalt is within the chemical and temporal ranges of the Cenozoic alkali basalts, some of which provided mantle xenoliths in the SW Japan arc (Figure 1). The position of Bankawa is very peculiar and very different from those of other Cenozoic alkali basalts, which carried mantle xenoliths, except for Shingu (Figure 1). The xenolith-bearing alkali basalt magmas erupted through a slab window that had been present between the Japan Sea (backarc basin) opening and the initiation of subduction of the Shikoku Basin (young part of the Philippine Sea plate) in Miocene [29,53]. The slab window is expected to be getting narrower with progress of the subduction, and the alkali basaltic magma that erupted on the Pacific side is old in age, such as that of Shingu (17 Ma) [30]. It is noteworthy that the Bankawa alkali basalt is almost coeval with the Noyamadake basanite (7.4 Ma) [29] on the Japan Sea side (Figure 1).

Geometrical analysis of subducting Philippine Sea plate by seismic tomography demonstrates that the subduction has not uniformly proceeded; the leading edge of the slab is very shallow and located beneath Osaka city around 50 km to the north of Bankawa (Figure 1) [28,96]. This is in contrast to the

other part of the SW Japan arc, where the leading edge of the slab has been close to the Quaternary volcanic front (Figure 1). Considering a spreading rate of the Philippine Sea plate (a few cm/year) and a medium angle of subduction, the Bankawa area was not possibly underlain by the slab when the alkali basalt erupted there (7.5 Ma). In other words, a slab window was still open then so that asthenospheric magma could move upward and erupt.

Some of the Bankawa lherzolite xenoliths contain secondary phlogopites (Figure 3f) and show variations of mineral chemistry closely related with the formation of phlogopite (Figures 6–9). The textural and chemical characters indicate that the Bankawa phlogopite is of metasomatic origin. The metasomatism by the melt that precipitated the phlogopite dramatically changed the chemical properties of the mantle minerals in the Bankawa lherzolite (see Section 6.1.2 above). Due to the metasomatic effects, olivine–spinel pairs in some phlogopite-bearing lherzolite are plotted off the olivine–spinel mantle array, the residual spinel peridotite trend [41] (Figure 8). Olivines were slightly enriched with Fe (Figures 6 and 8) and chromian spinels in a modally metasomatized (phlogopite-bearing) lherzolite (IZS-12) is slightly higher in Cr# and similar in composition to spinel inclusions in olivine phenocrysts of the host basalt (Figure 8). The metasomatism also enhanced the Na content of clinopyroxene (Figure 9), and dramatically changed trace-element contents of clinopyroxene. The calculated melt in equilibrium with the most metasomatized clinopyroxene (IZS-13) is similar in REE pattern to but more evolved than the host alkali basalt (Figure 13). The slight LREE enrichment of clinopyroxene in the phlogopite-free samples possibly represents incipient cryptic metasomatism.
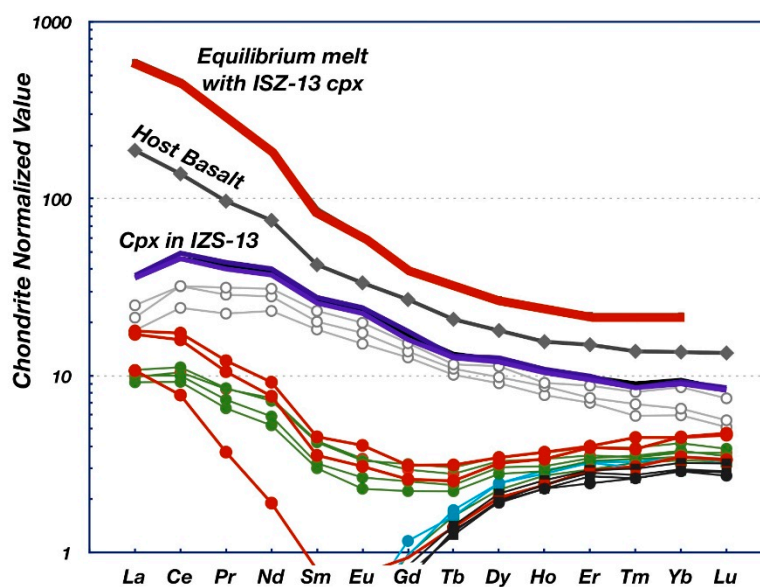
Figure 13. Chondrite-normalized REE pattern of the melt in equilibrium with clinopyroxene in a metasomatized Bankawa lherzolite, based on partition coefficients of Brunelli et al. [97]. The lherzolite (IZS-13) contains the clinopyroxene with the highest REE contents, and is expected to be the highest degree of metasomatism. Note the melt responsible for the metasomatism is very similar in REE pattern to the host alkali basalt.

Although the peridotites have been metasomatized to various degrees, no Group II xenolith and megacryst are associated with them. The least metasomatized one shows the enrichment only in LREE and some LILE (large-ion lithophile elements), but the most metasomatized one that shows the highest REE contents contains a modal metasomatic mineral, phlogopite, as well. The metasomatic agent is possibly an alkali basaltic melt similar in chemistry to the host rock. The formation of Ti-rich phlogopites is due to metasomatism by alkali basaltic melt, cogenetic with the host magma because the calculated melt in equilibrium with the clinopyroxene in the phlogopite-bearing lherzolite is similar to the host basalt in the REE pattern (Figure 13). This is consistent with the high-Ti character of Bankawa phlogopite, which is plotted within the field of phlogopites in continental rift-zone

peridotites metasomatized by asthenospheric alkali basaltic melt (Figure 10a). The metasomatic agent was not the host alkali basalt, which is free from phlogopite: the metasomatic features such as the presence of phlogopite are not related to the distance from the host basalt in the Bankawa xenoliths. The formation of phlogopite-rich veins (Figure 3f) is possibly representative of addition of Group II rocks in the upper mantle despite the absence of discrete Group II xenoliths in the Bankawa alkali basalt. It is noteworthy that the metasomatic addition of hydrous minerals to mantle peridotite has been observed only in the two most Pacific-ward localities, namely Shingu and Bankawa (Figure 1); Goto and Arai [82] reported Ti-rich pargasite and phlogopite as metasomatic minerals from the Shingu peridotites. This is in contrast to an almost anhydrous character of Group II xenoliths, of which the main mineral is Ti-rich clinopyroxene, from the other localities from the SW Japan arc [1]. The mantle diapirs involved in production of the Shingu and Bankawa alkali basalt magmas were possibly more hydrous than those responsible for the other continent-ward basalt activity in the Cenozoic. Nakamura et al. [51,52] interpreted the Cenozoic alkali basalts in the SW Japan arc as intraplate magmas with a slight arc-magma affinity, which suggests involvement of an asthenospheric mantle diapir chemically affected by fluid/melt derived from slab precedent to the current one. This is consistent with the relatively low-Ti character of chromian spinel in the Bankawa host basalt. The hydrous character of the most Pacific-ward diapirs for alkali basalt formation irrespective of the age (17 Ma for Shingu and 7.5 Ma for Bankawa) is due to selective hydration of a tip of the mantle wedge by a slab which had subducted before the initiation of the Japan Sea opening.

In summary, the Bankawa lherzolite has been metasomatized to various degrees by the melt that precipitated the phlogopite. The melt had an affinity to the host alkali basalt, and was produced slightly prior to the host magma from the same source mantle. The metasomatism started with enrichment only of REE and highly incompatible elements in clinopyroxene as in the case of IZS-1 and IZS-6 (Figure 11). With the appearance of modal phlogopite as in IZS-4, IZS-12 and IZS-13, all trace elements including HREE remarkably increase in clinopyroxene (Figue 11). The sample IZS-3 is transitional: it is free from modal phlogopite but its clinopyroxenes are variously enriched with trace elements (Figures 9 and 11). The metasomatizing agent for IZS-3 was possibly high in Na/K ratio due to fractionation during the metasomatism [71,98].

8.3. Origin of the Bankawa Lherzolite

The very limited lithological and chemical variations of the Bankawa lherzolite, apart from the metasomatic modification by alkali basalt, indicate a monotonous lherzolitic upper mantle near the tip of the mantle wedge beneath the SW Japan arc. This shows a strong contrast to the mantle of more continent-ward part of the SW Japan arc represented by xenoliths [1]. The unmetasomatized mantle peridotites from the SW Japan arc are substantially varied from a fertile lherzolite (e.g., Noyamadake and On-yama; spinel Cr# = 0.1) to a depleted harzburgite (Noyamadake; spinel Cr# = 0.7) [1,4,99,100]. They are very frequently accompanied by dunite-pyroxenites of Group I [1], suggesting a presence of thick "cumulus mantle", which comprises cumulative peridotites (mainly dunites and wehrlites) and pyroxenites [12]. In addition, Group II rocks have been added to both the mantle peridotite and the cumulative dunite-pyroxenites of Group I with chemical and petrographic modification to various extents [1].

The Bankawa lherzolite is similar in mineral chemistry to some abyssal lherzolite (Figures 8, 9 and 11). The former is equivalent to the latter in compositional ranges of olivine and chromian spinel (Figure 8). The REE pattern of Bankawa clinopyroxene strongly declines from HREE to Nd as in the abyssal peridotites (Figure 11), apart from the clear enrichment with LREE for the former, which is due to a cryptic incipient-stage metasomatism by alkali basaltic magma. The Na_2O content of unmetasomatized Bankawa clinopyroxenes is as low as that in typical abyssal lherzolites (Figure 9). The Bankawa lherzolite is possibly the peridotite initially formed at an oceanic ridge and subsequently trapped within the mantle wedge (Figure 14). It has escaped from partial melting to form arc magmas

or from reaction with other magmas passing through after initial entrapment in the mantle wedge (Figure 14).
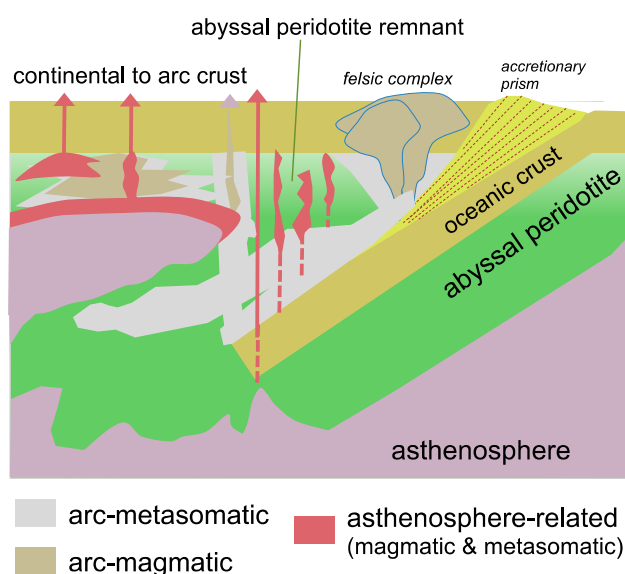
Figure 14. Cartoon to illustrate the evolution of mantle wedge after initiation of subduction. Arc-type magmas, slab-derived fluids and asthenospheric mgamas have modified the initial abyssal peridotite to various degrees through repeated subduction and break of slab after entrapment. The abyssal peridotite remnant, which has been devoid of the modification, is one of the important components of the mantle wedge.

9. Conclusions

The unmetasomatized peridotite from Bankawa is identical in pletrologic character to some abyssal lherzolites. It was trapped in the mantle wedge at an incipient stage of the (proto-) Japan arcs at the eastern margin of the Eurasian continent, and has escaped from later modification (partial melting and metasomatism) (Figure 14). Arai and Ishimaru [4,6] suggested that peridotites similar to the abyssal peridotite are present in the lithospheric mantle beneath the Japan arcs. Abe and Arai [99] reported that some peridotite xenoliths from the Japan arcs contain clinopyroxene depleted in LREE and are similar to the abyssal peridotite. The Japan island arcs have been on a subduction zone at the margin of the South China continental block since the Paleozoic (Cambrian) [100,101]. Peridotites initially formed at the mid-ocean ridge are one of the important components of the mantle wedge (Figure 14).

The Bankawa host alkali basalt was derived from the asthenosphere and passed through a slab window that was present beneath the Kii Peninsula due to the heterogeneous subduction of the Philippine Sea plate (Figure 1) [20,96]. The slab possibly had not reached beneath Bankawa when the alkali basalt erupted 7.5 Ma.

References

1. Arai, S.; Hirai, H.; Uto, K. Mantle peridotite xenoliths from the Southwest Japan arc and a model for the sub-arc upper mantle structure and composition of the Western Pacific rim. *J. Mineral. Petrol. Sci.* **2000**, *95*, 9–23. [CrossRef]

2. Arai, S.; Abe, N.; Ishimaru, S. Mantle peridotites from the Western Pacific. *Gondwana Res.* **2007**, *11*, 180–199. [CrossRef]

3. Nixon, P.H. (Ed.) *Mantle Xenoliths*; John Wiley & Sons: Chichester, UK, 1987; p. 844.

4. Arai, S.; Ishimaru, S. Insights into petrological characteristics of the lithosphere of mantle wedge beneath arcs through peridotite xenoliths: A review. *J. Petrol.* **2008**, *49*, 665–695. [CrossRef]

5. Kay, S.M.; Kay, R.W. Role of crystal cumulates and the oceanic crust in the formation of the lower crust of the Aleutian arc. *Geology* **1985**, *13*, 461–464. [CrossRef]

6. Arai, S.; Ishimaru, S. Petrologic characteristics of the upper mantle beneath island arcs. *J. Geol. Soc. Jpn.* **2018**, *124*, 551–573. (In Japanese) [CrossRef]

7. Boudier, F.; Nicolas, A.; Bouchez, J.L. Kinematics of oceanic thrusting and subduction from basalt sections of ophiolites. *Nature* **1982**, *296*, 825–828. [CrossRef]

8. Umino, S.; Yanai, S.; Jaman, A.P.; Nakamura, Y.; Iiyama, J.T. The transition from spreading to subduction: Evidence from the Semail ophiolite, northern Oman mountains. In *Ophiolites, Oceanic Crustal Analogures. Proceedings of the Symposium 'Troodos 1987'*; Malpas, J., Moores, E.M., Xenophontos, C., Eds.; Geological Survey Department: Nicosia, Cyprus, 1990; pp. 375–384.

9. Arai, S.; Kadoshima, K.; Morishita, T. Widespread arc-related melting in the mantle section of the northern Oman ophiolite as inferred from detrital chromian spinels. *J. Geol. Soc.* **2006**, *163*, 869–879. [CrossRef]

10. Le Mée, L.; Girardeau, J.; Monnier, C. Mantle segmentation along the Oman ophiolite fossil mid-ocean ridge. *Nature* **2004**, *432*, 167–172. [CrossRef] [PubMed]

11. Kanke, N.; Takazawa, E. A kilometer-scale highly refractory harzburgite zone in the mantle section of the northern Oman Ophiolite (Fizh Block): Implications for flux melting of oceanic lithosphere mantle. In *Tectonic Evolution of the Oman Mountains*; Rollinson, H., Searle, M.P., Abbasi, I.A., Al-Lazki, A., Al Kindi, M.H., Eds.; Geological Society: London, UK, 2014; pp. 229–246.

12. Takahashi, E. Petrlogical model of the crust and upper mantle of the Japanese island arcs. *Bull. Volcanol.* **1978**, *41*, 529–547. [CrossRef]

13. Takahashi, E. Genesis of calc-alkali andesite magma in a hydrous mantle-crust boundary: Petrology of lherzolite xenoliths from the Ichinomegata crater, Oga Peninsula, northeast Japan, part II. *J. Volcanol. Geotherm. Res.* **1986**, *29*, 355–395. [CrossRef]

14. Aoki, K. Japanese Island arc: Xenoliths in alkali basalts, high-alumina basalts, and calc-alkaline andesites and dacites. In *Mantle Xenoliths*; Nixon, P.H., Ed.; John Wiley & Sons: Chichester, UK, 1987; pp. 319–333.

15. Arai, S.; Hirai, H.; Abe, N. Geological aspects of peridotite and related xenoliths in volcanic rocks: An example from the Japan arcs. *Jpn. Mag. Mineral. Petrogical Sci.* **2005**, *34*, 133–142. (In Japanese)

16. Ishiwatari, A.; Ozawa, K.; Arai, S.; Ishimaru, S.; Abe, N.; Takeuchi, M. Ophiolites and ultramafic rocks. In *The Geology of Japan*; Moreno, T., Wallis, S.R., Kojima, T., Gibbons, W., Eds.; Geological Society: London, UK, 2016; pp. 223–250.

17. McInnes, B.I.A.; Grégoire, M.; Binns, R.A.; Herzig, P.M.; Hannington, M.D. Hydrous metasomatism of oceanic subarc mantle, Lihir, Papua New Guinea: Petrology and geochemistry of fluid-metasomatized mantle wedge xenoliths. *Earth Planet. Sci. Lett.* **2001**, *188*, 169–183. [CrossRef]

18. Franz, L.; Becker, K.-P.; Kramer, W.; Herzig, P.M. Metasomatic mantle xenoliths from Bismark microplate (Papua New Guinea)—Thermal evolution, geochemistry and extent of slab-induced metasomatism. *J. Petrol.* **2002**, *43*, 315–343. [CrossRef]

19. Ishimaru, S.; Arai, S.; Ishida, Y.; Shirasaka, M.; Okrugin, V.M. Melting and multi-stage metasomatism in the mantle wedge beneath a frontal arc inferred from highly depleted peridotite xenoliths from the Avacha volcano, southern Kamchatka. *J. Petrol.* **2007**, *48*, 395–433. [CrossRef]

20. Bloomer, S.H.; Hawkins, J.W. Gabbroic and ultramafic rocks from the Mariana trench: An island arc ophiolite. In *The Tectonic and Geologic Evolution of Southwest Asian Seas and Islands*; Hayes, D.E., Ed.; Geophysical Monograph 27; American Geophysical Union: Washington, DC, USA, 1983; pp. 294–317.

21. Ishii, T.; Robinson, P.T.; Maekawa, H.; Fiske, R. Petrological studies of peridotites from diapiric serpentinite semounts in the Izu-Ogasawara-Mariana forearc, Leg 125. *Proc. Ocean Drill. Program Sci. Results* **1992**, *125*, 445–485.

22. Ohara, Y.; Ishii, T. Peridotites from the southern Mariana forearc: Heterogeneous fluid supply in the mantle wedge. *Island Arc* **1989**, *7*, 541–558. [CrossRef]

23. Michibayashi, K.; Ohara, Y.; Stern, R.J.; Fryer, P.; Kimura, J.-I.; Tasaka, M.; Harigane, Y.; Ishii, T. Peridotites from a ductile shear zone within back-arc lithospheric mantle, southern Mariana Trench: Results of a *Shinkai 6500* dive. *Geochem. Geophys. Geosyst.* **2009**, *10*, Q05X06. [CrossRef]

24. Seike, K. The first record of intrusive alkali basalts in the Izumi Mountains, South Kinki district, Japan. *Bull. Saitama Museum Nat. Hist.* **2016**, *10*, 67–68. (In Japanese)

25. Tatsumi, Y. High-Mg andesites in the Setouchi Volcanic Belt, Southwest Japan: Analogy to Archean magmatism and continental crust formation? *Annu. Rev. Earth Planet. Sci.* **2006**, *34*, 457–499. [CrossRef]

26. Seike, K.; Hirano, H. Organic maturation and burial history models of the Upper Cretaceous Izumi Group in the Izumi Mounrtains, Southwest Japan. *J. Geol. Soc. Jpn.* **2013**, *119*, 397–409. (In Japanese) [CrossRef]

27. Kimura, J.-I.; Kunikiyo, T.; Osaka, I.; Nagao, T.; Yamauchi, S.; Kakubuchi, S.; Okada, S.; Fujibayashi, N.; Okada, R.; Murakami, H.; et al. Late Cenozoic volcanic activity in the Chugaoku area, southwest Japan arc during back-arc basin opening and reinitiation of subduction. *Island Arc* **2003**, *12*, 22–45. [CrossRef]

28. Nakajima, J.; Hasegawa, A. Subduction of the Philippine Sea plate benath southwestern Japan: Slab geometry and its relationship to arc magmatism. *J. Geophys. Res.* **2007**, *112*, B08306. [CrossRef]

29. Uto, K. Neogene Volcanism of Southwest Japan: Its Time and Space on K-Ar Dating. Ph.D. Thesis, University of Tokyo, Tokyo, Japan, 1990; p. 184.

30. Uto, K.; Hirai, H.; Goto, K.; Arai, S. K-Ar ages of carbonate- and mantle nodule-bearing lamprophyre dikes from Shingu, central Shikoku, Southwest Japan. *Geochem. J.* **1987**, *21*, 283–290. [CrossRef]

31. Kimura, J.-I.; Stern, R.J.; Yoshida, T. Reinitiation of subduction and magmatic responses in SW Japan during Neogene time. *Geol. Soc. Am. Bull.* **2005**, *117*, 969–986. [CrossRef]

32. Sakuyama, M. Cenozic volcanisms and mantle dynamics in Japan: Progress in the last 10 years. *J. Geogr.* **2010**, *119*, 1063–1078. (In Japanese) [CrossRef]

33. Seike, K.; Iwano, H.; Danhara, T.; Hirano, H. Tectonics of the Ryoke-Izumi belt of the Izumi Mountains, Southwest Japan from thermochronological data. *J. Geol. Soc. Jpn.* **2013**, *119*, 759–775. (In Japanese) [CrossRef]

34. Miyata, T. Wrench fault tectonics of the Median Tectonic Line and deformation of the Cretaceous Izumi Group in west Kinki, southwest Japan. *J. Geosci. Osaka City Univ.* **1980**, *23*, 65–114.

35. Sato, T. Volcanic rocks in Mt. Kabutoyama, Mt. Shigisan, Mt. Unebiyama, Mt. Dakeyama, and other regions. In *Geology of Japan, No.5: Kinki District*; Geological Society of Japan, Ed.; Asakura-Shoten: Tokyo, Japan, 2009; pp. 276–278. (In Japanese)

36. Miyata, T.; Makimoto, H.; Ichikawa, K.; Samukawa, A. *Geology of the Wakayama and Ozaki District: With Geological Sheet Map at 1:50000*; Geological Survey of Japan: Tsukuba, Japan, 1993; p. 68. (In Japanese)

37. Morozumi, Y. Late Cretaceous (Campanian and Maastrichtian) ammonites from Awaji Island, Southwest Japan. *Bull. Osaka Mus. Nat. Hist.* **1985**, *39*, 1–58.

38. Hirai, H. Mode of occurrence of alkali basaltic volcanic products and their inclusions of Noyamadake, Shimane Prefecture, southwestern Japan. *J. Jpn. Assoc. Mineral. Petrol. Econ. Geol.* **1983**, *78*, 211–220. (In Japanese) [CrossRef]

39. Arai, S.; Abe, N. Reaction of orthopyroxene in peridotite xenoliths with alkali basalt melt and its implication for genesis of alpine-type chromitite. *Am. Mineral.* **1995**, *80*, 1041–1047. [CrossRef]

40. Frey, F.A.; Prinz, M. Ultramafic inclusions from San Carlos, Arizona: Petrologic and geochemical data bearing on their petrogenesis. *Earth Planet. Sci. Lett.* **1978**, *38*, 129–176. [CrossRef]

41. Arai, S. Characterization of spinel peridotites by olivine-spinel compositional relationships: Review and interpretation. *Chem. Geol.* **1994**, *113*, 191–204. [CrossRef]

42. Morishita, T.; Ishida, Y.; Arai, S.; Shirasaka, M. Determination of multiple trace element compositions in thin (<30 μm) layers of NIST SRM 614 and 616 using laser ablation-inductively coupled plasma-mass spectrometry. *Geostand. Geoanal. Res.* **2005**, *29*, 107–122.

43. Tamura, A.; Akizawa, N.; Otsuka, R.; Kanayama, K.; Python, M.; Morishita, T.; Arai, S. Measurement of whole-rock trace-element composition by flux-free fused glass and LA-ICP-MS: Evaluation of simple and rapid routine work. *Geochem. J.* **2015**, *49*, 243–258. [CrossRef]

44. Jochum, K.P.; Nohl, U. Reference materials in geochemistry and environmental research and the GeoReM database. *Chem. Geol.* **2008**, *253*, 50–53. [CrossRef]

45. Longerich, H.P.; Jackson, S.E.; Gunther, D. Laser ablation inductively coupled plasma mass spectrometric transient signal data acquisition and analyte concentration calculation. *J. Anal. At. Spectrom.* **1996**, *11*, 899–904. [CrossRef]

46. Kusano, Y.; Umino, S.; Kobayashi, J.; Mizukami, T.; Okuno, M.; Arai, S. Quantitative analysis of major elements in igneous rocks with X-ray fluorescence spectrometer "ZSX primus II" using a 1: 10 dilution glass bead. *Sci. Rep. Kanazawa Univ.* **2014**, *58*, 31–44.

47. Pearce, N.J.G.; Perkins, W.T.; Westgate, J.A.; Gorton, M.P.; Jackson, S.E.; Neal, C.R.; Chenery, S.P. A compilation of new and published major and trace element data for NIST SRM 610 and NIST SRM 612 glass reference materials. *Geostand. Newslett.* **1997**, *21*, 115–144. [CrossRef]

48. Wells, P.R.A. Pyroxene thermometry in simple and complex systems. *Contrib. Mineral. Petrol.* **1977**, *62*, 129–139. [CrossRef]

49. Wood, B.J.; Banno, S. Garnet-orthopyroxene and orthopyroxene-clinopyroxene relationships in simple and complex systems. *Contrib. Mineral. Petrol.* **1973**, *42*, 109–124. [CrossRef]

50. Miyashiro, A. Nature of alkalic volcanic rock series. *Contrib. Mineral. Petrol.* **1978**, *66*, 91–104. [CrossRef]

51. Nakamura, E.; Campbell, I.H.; McCulloch, M.T.; Sun, S.-S. Chemical Geodynamics in a Back Arc Region Around the Sea of Japan: Implications for the Genesis of Alkaline Basalts in Japan, Korea, and China. *J. Geophys. Res.* **1989**, *94*, 4634–4654. [CrossRef]

52. Nakamura, E.; McCulloch, M.T.; Campbell, I.H. Chemical geodynamics in the back-arc region of Japan based on the trace element and Sr-Nd isotopic compositions. *Tectonophysics* **1990**, *174*, 207–233. [CrossRef]

53. Iwamori, H. Zonal structure of Cenozoic basalts related to mantle upwelling in Southwest Japan. *J. Geophys. Res.* **1991**, *96*, 6157–6170. [CrossRef]

54. Iwamori, H. Degree of melting and source composition of Cenozoic basalts in Southwest Japan: Evidence for mantle upwelling by flux melting. *J. Geophys. Res.* **1992**, *97*, 10983–10995. [CrossRef]

55. Uto, K.; Takahashi, E.; Nakamura, E.; Kaneoka, I. Geochronology of alkali volcanism in Oki-Dogo Island, Southwest Japan: Geochemical evolution of basalts related to the opening of the Japan Sea. *Geochem. J.* **1994**, *28*, 431–449. [CrossRef]

56. Sakuyama, T.; Ozawa, K.; Sumino, H.; Nagao, K. Progressive Melt Extraction from Upwelling Mantle Constrained by the Kita-Matsuura Basalts in NW Kyushu, SW Japan. *J. Petrol.* **2009**, *50*, 725–779. [CrossRef]

57. Kim, K.H.; Tanaka, T.; Nagao, K.; Jang, S.K. Nd and Sr isotopes and K-Ar ages of the Ulreungdo alkali volcanic rocks in the East Sea, South Korea. *Geochem. J.* **1999**, *33*, 317–341. [CrossRef]

58. Dostal, J.; Dupuy, C.; Zhai, M.; Zhi, X. Geochemistry and origin of Pliocene alkali basaltic lavas from Anhui-Jiangsu, eastern China. *Geochem. J.* **1988**, *22*, 165–176. [CrossRef]

59. Zou, H.; Zindler, A.; Xu, X.; Qi, Q. Major, trace element, and Nd, Sr and Pb isotope studies of Cenozoic basalts in SE China: Mantle sources, regional variations, and tectonic significance. *Chem. Geol.* **2000**, *171*, 33–47. [CrossRef]

60. Zhang, Z.; Feng, C.; Li, C.; Li, S.; Xin, Y.; Li, Z.; Wang, X. Petrochemical study of the Jingpohu Holocene alkali basaltic rocks, northeastern China. *Geochem. J.* **2002**, *36*, 133–153. [CrossRef]

61. Yan, J.; Zhao, J.-X. Cenozoic alkali basalts from Jingpohu, NE China: The role of lithosphere-asthenosphere interaction. *J. Asian Earth Sci.* **2008**, *33*, 106–121. [CrossRef]

62. Allan, J.F.; Gorton, M.P. Geochemistry of igneous rocks from Legs 127 and 128, Sea of Japan. *Proc. Ocean Drill. Program Sci. Results* **1992**, *127/128*, 905–929.

63. Pouclet, A.; Lee, J.-S.; Vidal, P.; Cousens, B.; Bellon, H. Cretaceous to Cenozoic volcanism in South Korea and in the Sea of Japan: Magmatic constraints on the opening of the back-arc basin. In *Volcanism Associated with Extension at Consuming Plate Margins*; Smellie, J.L., Ed.; Geological Society Special Publication 81; Geological Society: London, UK, 1995; pp. 169–191.

64. Takamura, H. Petrographical and petrochemical studies of the Cenozoic basaltic rocks in Chugoku Province. *Geol. Rep. Hiroshima Univ.* **1973**, *18*, 1–167. (In Japanese)

65. Sun, S.S.; McDonough, W.F. Chemical and isotopic systematics of oceanic basalts: Implications for mantle composition and processes. In *Magmatism in the Ocean Basins*; Saunders, A.D., Norry, M.J., Eds.; Geological Society Special Publication 42; Geological Society: London, UK, 1989; pp. 313–345.

66. Arai, S. Chemistry of chromian spinel in volcanic rocks as a potential guide to magma chemistry. *Mineral. Mag.* **1992**, *56*, 173–184. [CrossRef]

67. Arai, S. Compositional variation of olivine-chromian spinel in Mg-rich magmas as a guide to their residual spinel peridotites. *J. Volcanol. Geotherm. Res.* **1994**, *59*, 279–294. [CrossRef]

68. Shukuno, H.; Arai, S. Olivine-chromian spinel compositional relationships of the Cenozoic alkali basalts from Southwest Japan: Implications for their mantle restite. *J. Mineral. Petrol. Econ. Geol.* **1999**, *94*, 120–140. [CrossRef]

69. Takahashi, E. Origin of basaltic magmas-implications from peridotite melting experiments and olivine fractionation model. *Bull. Volcanol. Soc. Jpn.* **1986**, *30*, S17–S40. (In Japanese)

70. Arai, S. Petrological characteristics of the upper mantle peridotites beneath the Japan Island Arcs—Petrogenesis of spinel peridotites. *Sov. Geol. Geophys.* **1991**, *32*, 8–26.

71. Arai, S. K/Na variation in phlogopite and amphibole of upper mantle peridotites due to fractionation of the metasomatic fluids. *J. Geol.* **1986**, *94*, 436–444. [CrossRef]

72. Arai, S.; Takahashi, N. Formation and compositional variation of phlogopites in the Horoman peridotite complex, Hokkaido, northern Japan: Implications for origin and fractionation of metasomatic fluids in the upper mantle. *Contrib. Mineral. Petrol.* **1989**, *101*, 165–175. [CrossRef]

73. Arai, S. Pressure-temperature dependent compositional variation of phlogopitic micas in upper mantle peridotites. *Contrib. Mineral. Petrol.* **1984**, *87*, 260–264. [CrossRef]

74. Delaney, J.S.; Smith, J.V.; Carswell, D.A.; Dawson, J.B. Chemistry of micas from Kimberlites and xenoliths-II. Primary- and secondary-textured micas from peridotite xenoliths. *Geochim. Cosmochim. Acta* **1980**, *44*, 857–872. [CrossRef]

75. Francis, D.M. The origin of amphibole in lherzolite xenoliths from Nunivak Island, Alaska. *J. Petrol.* **1976**, *17*, 357–378. [CrossRef]

76. Griffin, W.L.; Wass, S.Y.; Hollis, J.D. Ultramasic xenoliths from Bullenmerri and Gnotuk Maars, Victoria, Australia: Petrology of a sub-continental crust-mantle transition. *J. Petrol.* **1984**, *25*, 53–87. [CrossRef]

77. Ionov, D.A.; Ashchepkov, I.V.; Stosch, H.-G.; Witt-Eickschen, G.; Seck, H.A. Garnet peridotite xenoliths from the Vitim volcanic field, Baikal region: The nature of the garnet-spinel peridotite transition zone in the continental mantle. *J. Petrol.* **1993**, *34*, 1141–1175. [CrossRef]

78. Kida, M. Peridotite Xenoliths from Iraya Volcano, the Philippines: Metasomatized Peridotite Beneath the Immature arc. Master's Thesis, Kanazawa University, Kanazawa, Japan, 1998; p. 78. (In Japanese)

79. Xu, Y.-G.; Bodinier, J.-L. Contrasting enrichments in high- and low-temperature mantle xenoliths from Nushan, eastern China: Results of a single metasomatic event during lithospheric accretion? *J. Petrol.* **2004**, *45*, 321–341. [CrossRef]

80. Zhang, M.; Suddaby, P.; O'Reilly, S.Y.; Norman, M.; Qiu, J. Nature of the lithospheric mantle beneath the eastern part of the Central Asian fold belt: Mantle xenolith evidence. *Tectonophysics* **2001**, *328*, 131–156. [CrossRef]

81. Arai, S.; Takahashi, N. Phlogopites in solid intrusive peridotites: Their modes of occurrence and chemical characteristics. *Sci. Rep. Inst. Geosci. Univ. Tsukuba Ser.* **1987**, *8*, 75–92.

82. Goto, K.; Arai, S. Petrology of peridotite xenoliths in lamprophyre from Shingu, Southwestern Japan: Implications for origin of Fe-rich mantle peridotite. *Mineral. Petrol.* **1987**, *37*, 137–155. [CrossRef]

83. Kelemen, P.B.; Johnson, K.T.P.; Kinzler, R.J.; Irving, A.J. High-field-strength element depletions in arc basalts due to mantle-magma interaction. *Nature* **1990**, *345*, 521–524. [CrossRef]

84. Brunelli, D.; Cipriani, A.; Ottolini, L.; Peyve, A.; Bonatti, E. Mantle peridotites from the Bouvet Triple Junction Region, South Atlantic. *Terra Nova* **2003**, *15*, 194–203. [CrossRef]

85. Tamura, A.; Arai, S.; Ishimaru, S.; Andal, E.S. Petrology and geochemistry of peridotites from IODP Site U1309 at Atlantic Massif, MAR 30 °N: Micro- and macro-scale melt penetrations into peridotites. *Contrib. Mineral. Petrol.* **2008**, *155*, 491–509. [CrossRef]

86. Johnson, K.T.M.; Dick, H.J.B.; Shimizu, N. Melting in the oceanic upper mantle: An ion microprobe study of diopsides in abyssal peridotites. *J. Geophys. Res.* **1990**, *95*, 2661–2678. [CrossRef]

87. Johnson, K.T.M.; Dick, H.J.B. Open system melting and temporal and spatial variation of peridotite and basalt at the Atlantis II Fracture Zone. *J. Geophys. Res.* **1992**, *97*, 9219–9241. [CrossRef]

88. Hellebrand, E.; Snow, J.E.; Hoppe, P.; Hofmann, A. Garnet-field melting and late-stage refertilization in 'residual' abyssal peridotites from the Central Indian Ridge. *J. Petrol.* **2002**, *43*, 2305–2338. [CrossRef]

89. Rampone, E.; Bottazzi, P.; Ottolini, L. Complementary Ti and Zr anomalies in orthopyroxene and clinopyroxene from mantle peridoties. *Nature* **1991**, *354*, 518–520. [CrossRef]

90. Ballhaus, C.; Berry, R.F.; Green, D.H. High pressure experimental calibration of the olivine-orthopyroxene-spinel oxygen geobarometer: Implications for the oxidation state of the upper mantle. *Contrib. Mineral. Petrol.* **1991**, *107*, 27–40. [CrossRef]

91. Noda, A. Forearc basins: Types, geometries, and relationships to subduction zone dunamics. *Geol. Soc. Am. Bull.* **2016**, *128*, 879–895. [CrossRef]

92. Tatsumi, Y.; Ishikawa, N.; Anno, K.; Ishizaka, K.; Itaya, T. Tectonic setting of high-Mg andesite magmatism in the SW Japan arc: K-Ar chronology of the Setouchi volcanic belt. *Geophys. J. Int.* **2001**, *144*, 625–631. [CrossRef]

93. Nakajima, T.; Takahashi, M.; Imaoka, T.; Shimura, T. Granitic rocks. In *The Geology of Japan*; Moreno, T., Wallis, S.R., Kojima, T., Gibbons, W., Eds.; Geological Society: London, UK, 2016; pp. 251–272.

94. Wallis, S.R.; Okudaira, T. Paired metamorphic belts of SW Japan: The geology of the Sanbagawa and Ryoke metamorphic belts and the Median Tectonic Line. In *The Geology of Japan*; Moreno, T., Wallis, S.R., Kojima, T., Gibbons, W., Eds.; Geological Society: London, UK, 2016; pp. 101–124.

95. Takamura, H. Finding of spinel-lherzolite xenolith in basaltic sheets from Shingu, Ehime Prefecture, Japan. *J. Geol. Soc. Jpn.* **1978**, *84*, 475–479. (In Japanese) [CrossRef]

96. Nakajima, J.; Hasegawa, A. Tomographic evidence for the mantle upwelling beneath southwestern Japan and its implications for arc magmatism. *Earth Planet. Sci. Lett.* **2007**, *254*, 90–105. [CrossRef]

97. Brunelli, D.; Seyler, M.; Cipriani, A.; Ottolini, L.; Bonatti, E. Discontinuous melt extraction and weak refertilization of mantle peridotites at the Vema lihtospheric section (Mid-Atlantic Ridge). *J. Petrol.* **2006**, *47*, 745–771. [CrossRef]

98. Arai, S.; Matsukage, K.; Isobe, E.; Vysotskiy, S. Concentration of incompatible elements in oceanic mantle: Effect of melt/wall interaction in stagnant or failed conduits within peridotite. *Geochim. Cosmochim. Acta* **1997**, *61*, 671–675. [CrossRef]

99. Abe, N.; Arai, S. Petrography and geochemistry of the mantle xenoliths: Implications for lithospheric mantle beneath the Japan arcs. *J. Mineral. Petrol. Econ. Geol.* **2005**, *34*, 145–158. (In Japanese)

100. Cocks, R.L.M.; Torsvik, T.H. The dynamic evolution of the Paleozoic geography of eastern Asia. *Earth-Sci. Rev.* **2013**, *117*, 40–79. [CrossRef]

101. Taira, A.; Ohara, Y.; Wallis, S.R.; Ishiwatari, A.; Iryu, Y. Geological evolution of Japan: An overview. In *The Geology of Japan*; Moreno, T., Wallis, S.R., Kojima, T., Gibbons, W., Eds.; Geological Society: London, UK, 2016; pp. 1–24.